

RESEARCH ARTICLE

Targeting CD39 in Cancer Reveals an Extracellular ATP- and Inflammasome-Driven Tumor Immunity



Xian-Yang Li¹, Achim K. Moesta², Christos Xiao³, Kyohei Nakamura¹, Mika Casey¹, Haiyan Zhang¹, Jason Madore¹, Ailin Lepletier¹, Amelia Roman Aguilera¹, Ashmitha Sundarajan⁴, Celia Jacobberger-Foissac³, Clifford Wong², Tracy dela Cruz², Megan Welch², Alana G. Lerner², Bradley N. Spatola², Vanessa B. Soros², John Corbin², Ana C. Anderson⁵, Maïke Effern^{6,7,8}, Michael Hölzel^{6,7}, Simon C. Robson⁹, Rebecca L. Johnston¹⁰, Nicola Waddell¹⁰, Corey Smith¹¹, Tobias Bald⁴, Nishamol Geetha¹, Courtney Beers², Michele W. L. Teng³, and Mark J. Smyth¹

ABSTRACT

We explored the mechanism of action of CD39 antibodies that inhibit ectoenzyme CD39 conversion of extracellular ATP (eATP) to AMP and thus potentially augment eATP-P2-mediated proinflammatory responses. Using syngeneic and humanized tumor models, we contrast the potency and mechanism of anti-CD39 mAbs with other agents targeting the adenosinergic pathway. We demonstrate the critical importance of an eATP-P2X7-ASC-NALP3-inflammasome-IL18 pathway in the antitumor activity mediated by CD39 enzyme blockade, rather than simply reducing adenosine as mechanism of action. Efficacy of anti-CD39 activity was underpinned by CD39 and P2X7 coexpression on intratumor myeloid subsets, an early signature of macrophage depletion, and active IL18 release that facilitated the significant expansion of intratumor effector T cells. More importantly, anti-CD39 facilitated infiltration into T cell-poor tumors and rescued anti-PD-1 resistance. Anti-human CD39 enhanced human T-cell proliferation and Th1 cytokine production and suppressed human B-cell lymphoma in the context of autologous Epstein-Barr virus-specific T-cell transfer.

SIGNIFICANCE: Overall, these data describe a potent and novel mechanism of action of antibodies that block mouse or human CD39, triggering an eATP-P2X7-inflammasome-IL18 axis that reduces intratumor macrophage number, enhances intratumor T-cell effector function, overcomes anti-PD-1 resistance, and potentially enhances the efficacy of adoptive T-cell transfer.

¹Immunology in Cancer and Infection Laboratory, QIMR Berghofer Medical Research Institute, Herston, Queensland, Australia. ²Tizona Therapeutics, San Francisco, California. ³Cancer Immunoregulation and Immunotherapy Laboratory, QIMR Berghofer Medical Research Institute, Herston, Queensland, Australia. ⁴Oncology and Cellular Immunology Laboratory, QIMR Berghofer Medical Research Institute, Herston, Queensland, Australia. ⁵Harvard Medical School and Brigham and Women's Hospital, Boston, Massachusetts. ⁶Unit of RNA Biology, Department of Clinical Chemistry and Clinical Pharmacology, University Hospital Bonn, University of Bonn, Bonn, Germany. ⁷Institute of Experimental Oncology (IEO), University Hospital Bonn, University of Bonn, Bonn, Germany. ⁸Department of Microbiology and Immunology, The University of Melbourne at the Peter Doherty Institute for Infection and Immunity, Melbourne, Victoria, Australia. ⁹Departments of Medicine and Anesthesia, Beth Israel Deaconess Medical Center, Boston, Massachusetts. ¹⁰Medical Genomics Laboratory,

QIMR Berghofer Medical Research Institute, Herston, Queensland, Australia. ¹¹Translational and Human Immunology Laboratory, QIMR Berghofer Medical Research Institute, Herston, Queensland, Australia.

Note: Supplementary data for this article are available at Cancer Discovery Online (<http://cancerdiscovery.aacrjournals.org/>).

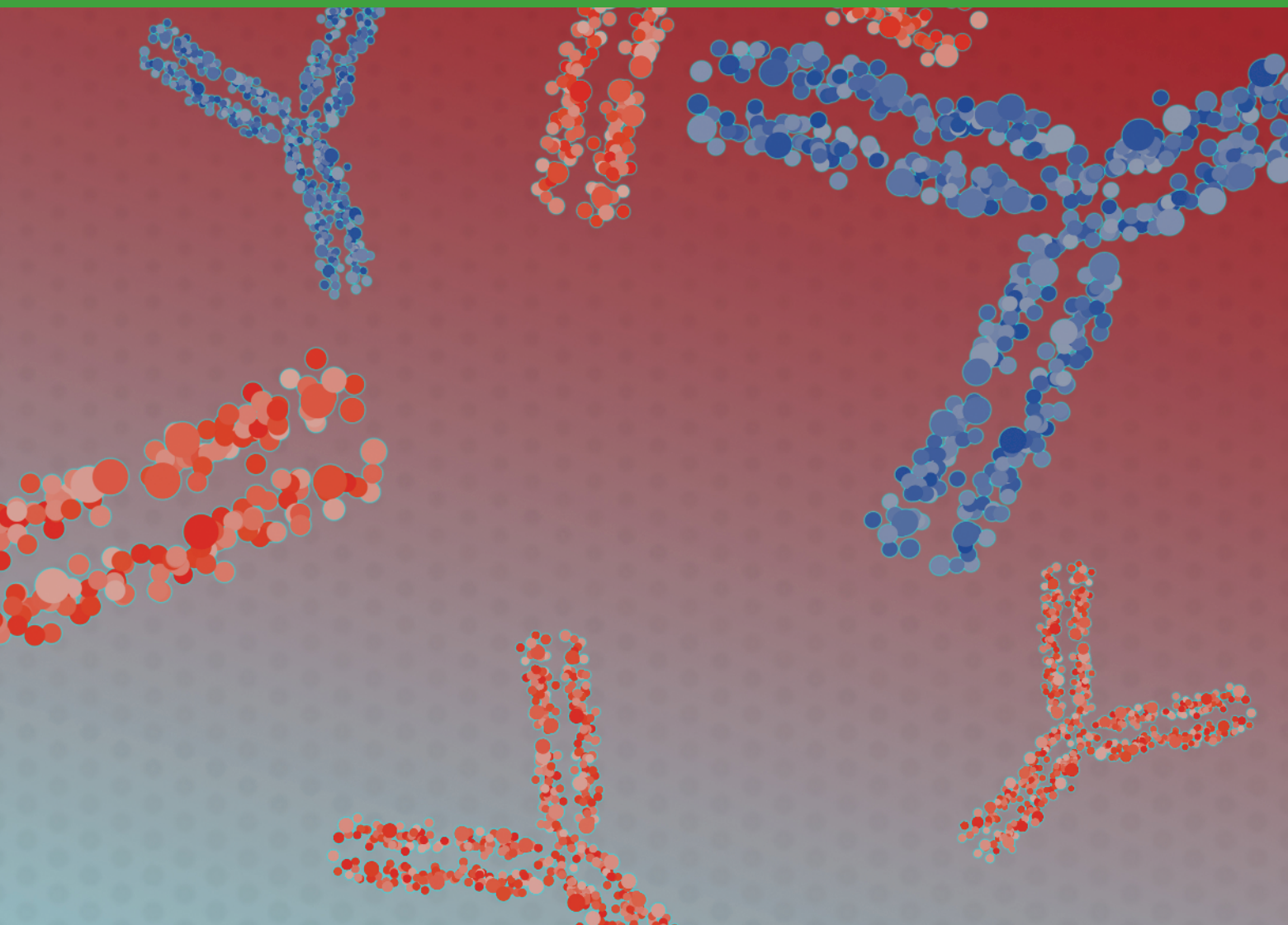
X.-Y. Li and A.K. Moesta contributed equally to this work.

Corresponding Author: Mark J. Smyth, QIMR Berghofer Medical Research Institute, 300 Herston Road, Herston, Queensland 4006, Australia. Phone: 617-3845-3957; Fax: 617-3362-0111; E-mail: Mark.Smyth@qimrberghofer.edu.au

Cancer Discov 2019;9:1754-73

doi: 10.1158/2159-8290.CD-19-0541

©2019 American Association for Cancer Research.



INTRODUCTION

Immune-checkpoint blockade (ICB) using antagonistic antibodies to CTLA4, PD-1, and PD-L1 has revolutionized the cancer treatment paradigm (1). However, despite the unprecedented responses achieved among select “immunogenically hot” tumor types with these therapies, the majority of patients still fail to achieve clinically relevant responses in those indications, and several tumor types show profound resistance to ICB (2). In addition, a significant proportion of patients who initially demonstrate antitumor responses following ICB therapy eventually become refractory and experience tumor relapse (3). Taken together, these observations reveal the need for additional immunotherapeutics and suggest that additional immune-escape mechanisms remain to be uncovered.

Although a multitude of clinical agents have entered the clinic as single agents or combination therapies with established ICBs, the majority of these fall into two categories: antagonists of additional immune checkpoints (e.g., LAG3, TIM3, and TIGIT) and agonists of costimulatory molecules (e.g., GITR, OX40, and 4-1BB). Altering the tumor microenvironment (TME)

by targeting tumor metabolic processes, such as the ATP–adenosine axis, is a new and promising avenue for therapeutic invention.

Purinergic signaling in the TME plays a key role in the regulation of immune responses. In solid tumors, ATP is abundantly released in the extracellular space owing to cell death in the tumor core, metabolic and/or hypoxic stress, and proinflammatory signals that stimulate active export of ATP, leading to an accumulation of extracellular ATP (eATP) levels far in excess of those found in healthy tissues (4, 5). eATP acts as a proinflammatory stimulus by agonizing P2 purinergic receptors (e.g., P2X7) on immune cells (6). However, tumors are proficient at scavenging eATP, converting it to immunosuppressive adenosine by means of two ectonucleotidases, CD39 and CD73, expressed on malignant cells, regulatory immune cells, and the vasculature (7). Adenosine exerts its suppressive function directly by binding to A2A receptors on multiple immune cells such as phagocytes, dendritic cells (DC), natural killer (NK) cells, T cells, and B cells (8–14). By controlling the initial steps in the phosphohydrolytic cascade, CD39 acts as the master regulator of this dynamic balance between proinflammatory

eATP and immunosuppressive adenosine within the TME, and thereby fosters a broadly immunosuppressive milieu (6).

In addition to elevated expression levels of CD39 in blood neoplasias and multiple solid-tumor settings (15–17), CD39 is broadly expressed on the vasculature and specifically found on certain immune subsets, including B cells, NK cells, DCs, monocytes, macrophages, and regulatory T cells (Treg; ref. 18). Within the TME, CD39 expression on Tregs (19, 20) and myeloid-derived suppressor cells (21, 22) has been shown to be directly correlated with the ability of these professional immunoregulatory cells to suppress T-cell function. CD8⁺ T cells, which show little detectable CD39 in peripheral blood, express significantly elevated CD39 levels across multiple human tumor types, including gastric cancer, renal cell carcinoma, non-small cell lung carcinoma (NSCLC), head and neck squamous cell carcinoma, breast cancer, and melanoma (23, 24). This apparent upregulation is accompanied by reduced polyfunctionality and induction of T-cell exhaustion signatures (24, 25). Recent reports also suggest that CD39 is a marker of tumor-reactive effector T-cell subsets (25, 26) and is increasingly appreciated as a regulatory marker (27).

The impact of CD39 on tumor growth and antitumor immunity has mostly been delineated using global CD39 gene-targeted mice; published data suggested that growth of multiple syngeneic tumors was reduced in these mice (28, 29). Similarly, CD39-deficient mice display a resistance to the formation of metastasis in models of disseminated disease or spontaneous metastasis formation (30, 31). In addition to genetic ablation, several reports from our laboratory and others have utilized the pharmacologic blockade of CD39 activity with the broad ectonucleotidase inhibitor sodium polyoxotungstate (POM1) to demonstrate improved antitumor immunity and decreased metastatic burden in preclinical models (30, 31). Additionally, Bastid and colleagues (32) demonstrated that *in vitro* treatment with POM1 reversed the suppression of T cells during coculture with CD39⁺/CD73⁺ melanoma cell lines.

Agents targeting other players in the adenosine pathway are currently undergoing clinical testing, including small-molecule

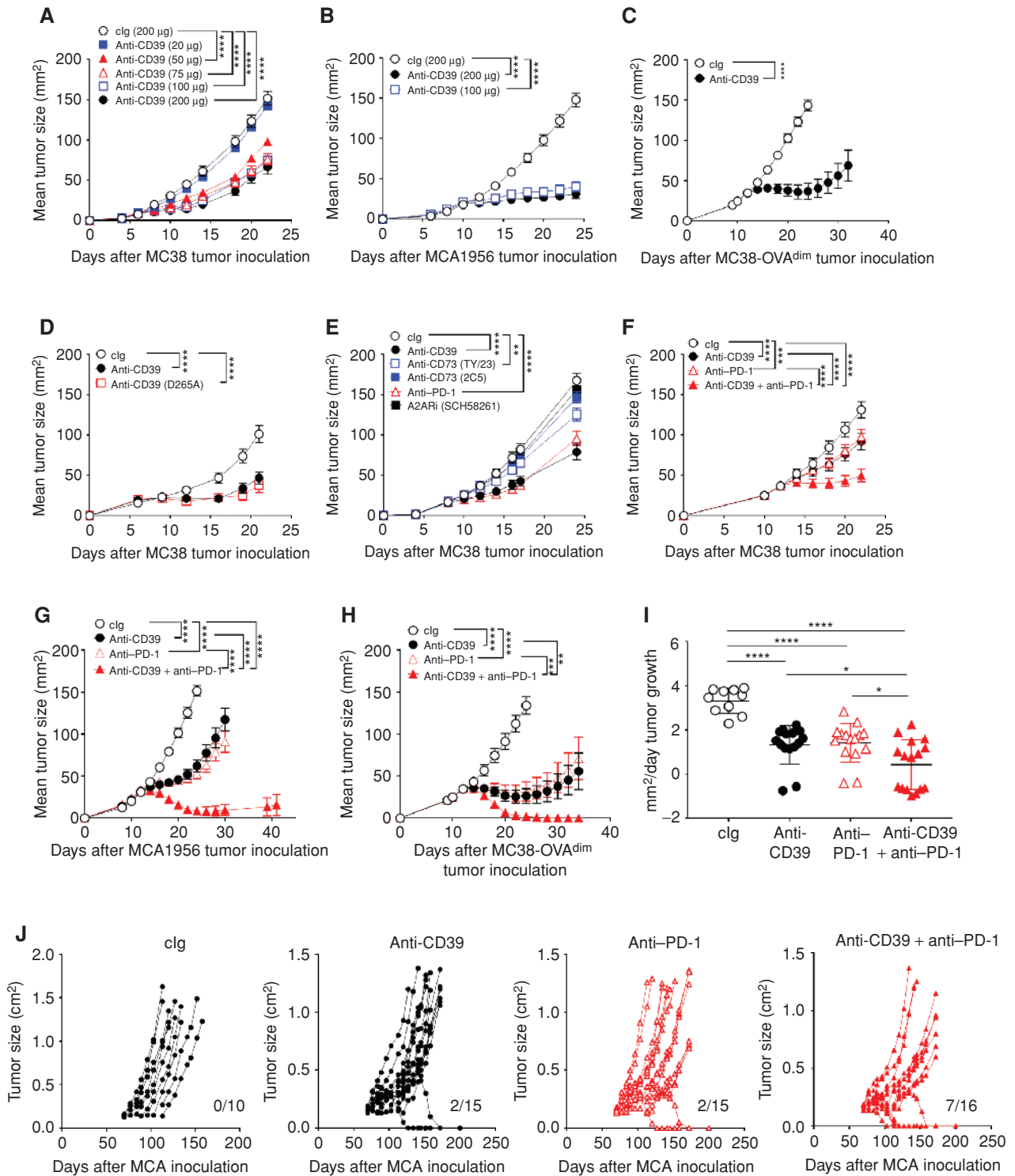
inhibitors of A2AR and antagonistic antibodies against CD73. An outstanding question has been whether targeting CD39 offers any therapeutic advantage by targeting a different mechanism of action than these other approaches. Here we report the use of novel antibodies that selectively block the enzymatic function of CD39 in mouse and human. We use these to determine that targeting CD39 may be a more potent approach by virtue of the unique eATP-P2X7-inflammasome-IL18 mechanism of action that reduces intratumor macrophages and enhances CD8⁺ T-cell effector function in the TME. In particular, we provide differentiation between therapeutic antibodies targeting CD39 and agents targeting other components of the adenosinergic system. Finally, we demonstrate the therapeutic potential of targeting CD39 in solid tumors, either as monotherapy or in potential ICB combinations, where anti-PD-1 alone was not effective.

RESULTS

Efficacy of Anti-Mouse CD39 mAb Monotherapy

Despite the fact that pharmacologic inhibitors of CD39, such as POM1, have previously been described to have potent antitumor activity (30, 31), questions around specificity, therapeutic half-life, pharmacokinetics, and toxicity have always left doubts about using this approach to target CD39. Effective anti-mouse CD39 mAb reagents have been lacking, in particular a mAb that allosterically inhibits CD39. We created a novel anti-mouse CD39 antibody, which specifically binds to CD39-expressing cells (Supplementary Fig. S1A) and potently inhibits CD39 ATPase activity *in vitro* (Supplementary Fig. S1B). This antibody (designated B66) was first tested against subcutaneous MC38 colon adenocarcinoma tumors, because this model is considered a standard and demonstrated by many laboratories as anti-PD-1-sensitive and immunogenic (33–35). Using a four-dose treatment schedule initiating once tumors were established, anti-CD39 was demonstrated to have potent single-agent activity against MC38 with efficacy at 50 to 200 μg doses, but significantly reduced activity at 20 μg doses (Fig. 1A). Similarly, 100 and 200 μg dose

Figure 1. Anti-CD39 suppresses established subcutaneous tumors. **A**, Anti-CD39 mAb suppresses MC38 tumor growth in a dose-dependent manner. Groups ($n = 5/\text{group}$) of WT mice were injected subcutaneously with MC38 (1×10^5) colon adenocarcinoma cells on day 0 and treated intraperitoneally with clg (200 μg) or anti-CD39 mAb (200, 100, 75, 50, or 20 μg) on days 7, 10, 13, and 16. Tumor sizes were measured at indicated time points in the graph, and data are presented as mean \pm SEM. This experiment is similar to two performed. **B**, Anti-CD39 mAb suppresses MCA1956 tumor growth in a dose-dependent manner. Groups ($n = 10/\text{group}$) of WT mice were injected subcutaneously with MCA1956 (1×10^6) fibrosarcoma cells on day 0 and treated intraperitoneally with clg (200 μg) or anti-CD39 (200 and 100 μg) on days 10, 13, 16, and 19. **C**, Anti-CD39 mAb suppresses MC38-OVA^{dim} tumor growth. Groups ($n = 10/\text{group}$) of WT mice were injected subcutaneously with MC38-OVA^{dim} (1×10^6) colon adenocarcinoma cells on day 0 and treated intraperitoneally with clg (200 μg) or anti-CD39 (200 μg) on days 12, 15, 18, and 21. **D**, Fc receptor-independent efficacy of anti-CD39 mAb. Groups ($n = 10/\text{group}$) of WT mice were injected subcutaneously with MC38 (1×10^5) colon adenocarcinoma cells on day 0 and treated intraperitoneally with clg (200 μg) or anti-CD39 (B66 or B66-D265A, 200 μg each) on days 6, 9, 12, and 15. **E**, Anti-CD39 mAb compared with other adenosine pathway inhibitors. Groups ($n = 7-10/\text{group}$) of WT mice were injected subcutaneously with MC38 (1×10^5) colon adenocarcinoma cells on day 0 and treated intraperitoneally with clg (200 μg), anti-CD39 (200 μg), anti-CD73 (2C5 or Ty/23, 200 μg), A2ARi (SCH58261, 10 mg/kg), or anti-PD-1 (250 μg) on days 8, 11, 14, and 17. This experiment is representative of two performed. **F**, Delayed suboptimal anti-CD39 and anti-PD-1 combination inhibited MC38 tumor growth. Groups ($n = 10/\text{group}$) of WT mice were injected subcutaneously with MC38 (1×10^5) colon adenocarcinoma cells on day 0 and treated intraperitoneally with clg (200 μg), anti-CD39 (100 μg), anti-PD-1 (100 μg), or combination of anti-CD39 and anti-PD-1 (100 μg each) on days 12, 15, 18, and 21. **G**, Suboptimal anti-CD39 and anti-PD-1 suppress MCA1956 tumor growth. Groups ($n = 10/\text{group}$) of WT mice were injected subcutaneously with MCA1956 (1×10^6) fibrosarcoma cells on day 0 and treated intraperitoneally with clg (100 μg I-536; 50 μg clone I-I), anti-CD39 (100 μg), anti-PD-1 (50 μg), combination of anti-CD39 and anti-PD-1 (100 μg; 50 μg) on days 12, 15, 18, and 21. **H**, Suboptimal anti-CD39 and anti-PD-1 cause rejection of MC38-OVA^{dim} tumors. Groups ($n = 10/\text{group}$) of WT mice were injected subcutaneously with MC38-OVA^{dim} (1×10^6) colon adenocarcinoma cells on day 0 and treated intraperitoneally with clg (100 μg mlgG1; 50 μg clone I-I), anti-CD39 (100 μg), anti-PD-1 (50 μg), combination of anti-CD39 and anti-PD-1 (100 μg; 50 μg) on days 12, 16, 20, and 24. **I** and **J**, Anti-CD39 and anti-PD-1 combine to reject *de novo* MCA-induced fibrosarcomas. Groups of WT mice ($n = 10-16/\text{group}$) were inoculated subcutaneously in the hind flank with MCA (300 μg) in 0.1 mL of corn oil and treated intraperitoneally with clg (100 μg), anti-CD39 (100 μg), anti-PD-1 (100 μg), or anti-CD39/anti-PD-1 (100 μg; 100 μg) twice/week for 6 weeks from the second palpable tumor measurement. All the mice were monitored for fibrosarcoma development for 250 days, and tumor growth rate (mm²/day; **I**) or individual tumor growth curves (**J**) are presented. Numbers in parentheses indicate the number of mice that rejected their tumors. Tumor sizes (mm² or cm²) were measured at the indicated time points and presented as mean \pm SEM. All experiments were performed once unless indicated. Significant differences among treatment groups were determined by a two-way ANOVA, followed by Tukey multiple-comparisons test (*, $P < 0.05$; **, $P < 0.01$; ***, $P < 0.001$; ****, $P < 0.0001$).



schedules of anti-CD39 were equivalently effective against the anti-PD-1-sensitive MCA1956 fibrosarcoma cell line (Fig. 1B), and the anti-CD39 monotherapy (200 μ g schedule) was also very effective against MC38-OVA^{dim} tumors (Fig. 1C). As determined by enzyme histochemistry, MC38 tumors displayed reduced ATPase activity 2 days after a single injection of mice with anti-CD39 compared with control Ig (cIg; Supplementary Fig. S2A and S2B). To illustrate that the activity of anti-CD39 (B66) was mediated by CD39 ectoenzyme blockade, two additional IgG1 anti-mouse CD39 mAbs (designated Tz-617 and Tz-619) that bound CD39 with similar affinity but lacked CD39 ectoenzyme blocking activity were shown to be ineffective against MC38 tumors (Supplementary Fig. S2C). To determine that the activity of anti-CD39 (B66) was mediated by CD39 binding rather than Fc activity, we mutated the FcR and compared mouse IgG1 and mouse IgG1 D265A variants of anti-CD39. Clearly, the Fc-mutant anti-CD39 (B66) was as potent as the intact IgG1 (B66) *in vivo* against MC38 tumors (Fig. 1D).

Using the MC38 tumor model, we next compared the monotherapeutic activity of anti-CD39 versus other described mAbs and inhibitors that block CD39 and other molecules in the adenosine pathway, including CD73 and adenosine A2A receptor (A2AR). Here we observed that anti-CD39 was as potent as anti-PD-1 (RMP-14), and other inhibitors and antibodies to CD73, A2AR, and CD39 were not nearly as effective as anti-CD39 monotherapy in this model (Fig. 1E; Supplementary Fig. S3A). Activities of anti-CD73 (2C5) and A2ARi (SCH58261) were observed against MC38 when used in combination with anti-CD39, but the majority of antitumor activity in these combinations was anti-CD39 mediated (Supplementary Fig. S3B). Even when using a combination of two anti-CD73 antibodies, A2ARi (SCH58261) or A2BRi (PSB1115) in the appropriate *Nt5e* (*Cd73*)^{-/-}, *Adora2a*^{-/-}, and *Adora2b*^{-/-} strain of mice from the time of tumor inoculation, anti-CD39 retained significant antitumor activity in such treated mice (Supplementary Fig. S4A–S4D). Indeed, the antitumor effect of anti-CD39 was greater than complete blockade of adenosine generation by CD73 and adenosine signaling via A2AR and A2BR, in both the MC38 and MCA1956 tumor models, but greatest tumor-growth inhibition was noted when all these molecules were collectively targeted.

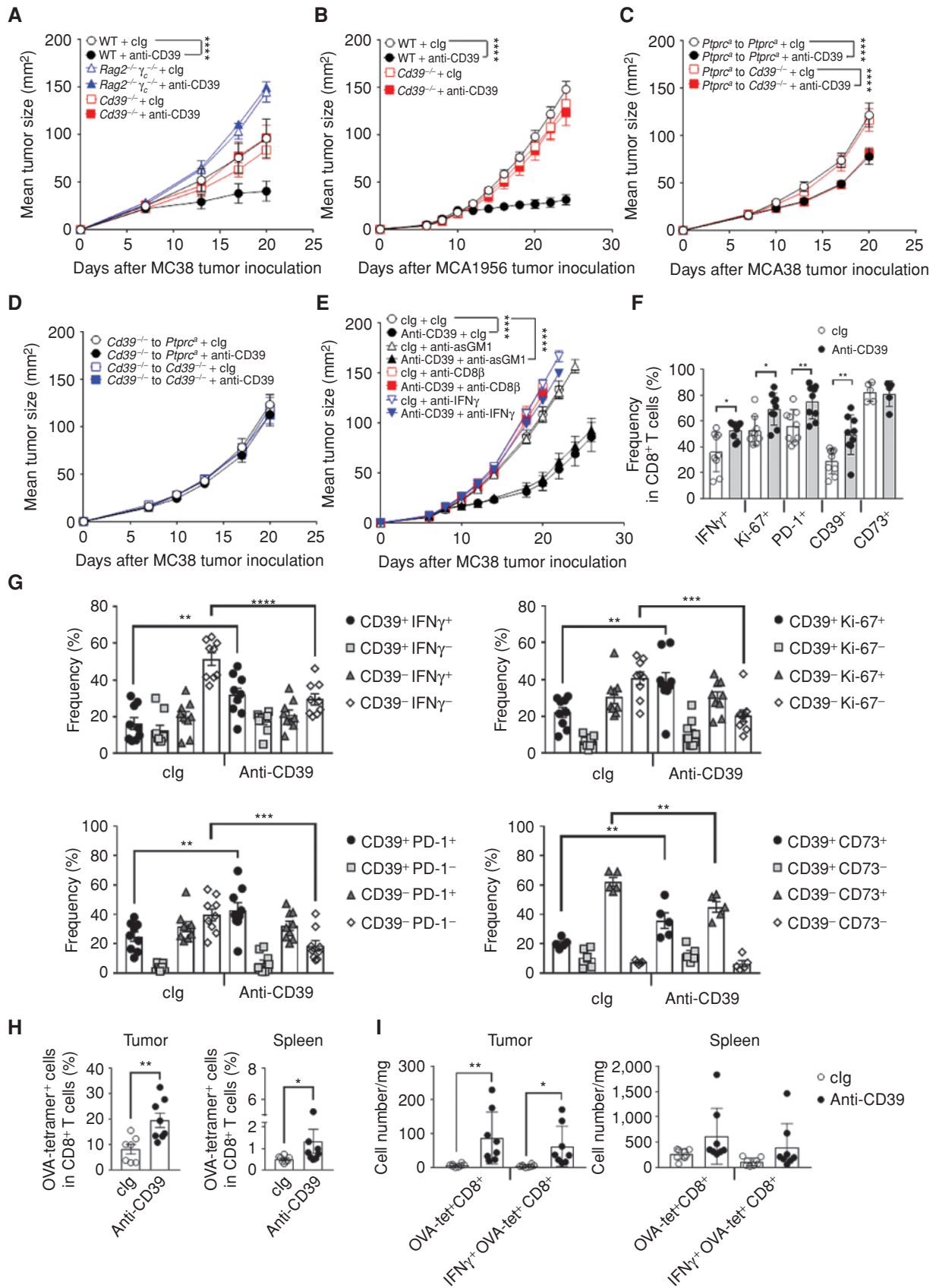
Combination Anti-PD-1 and Anti-CD39 mAb Antitumor Efficacy

We next evaluated the combination of suboptimal doses of anti-CD39 and anti-PD-1 in a delayed treatment setting using a series of tumor models that were responsive to PD-1 blockade (Fig. 1F–H). In each case, significant combination activity was observed between anti-CD39 and anti-PD-1, with many combination-treated mice completely rejecting MCA1956 and MC38-OVA^{dim} tumors (Supplementary Fig. S5A and S5B). Activity in immunogenic transplant models was encouraging, but it was not clear if anti-CD39 would be as effective in a *de novo* tumor setting where the tumor and immune system had co-evolved. We have previously published treatment in the MCA-induced fibrosarcoma model, and these established tumors prove an interesting model of tumor immunity because a spectrum of immunotherapeutic responses can be demonstrated against these tumors—from almost no response to complete rejection (36–38). Historically, effective combinations have demonstrated activity in a fraction of mice. Consistent with these findings, we found anti-PD-1 and anti-CD39 do have modest single-agent antitumor activity, displaying some slowing of tumor growth post-treatment compared with cIg and a low number of complete rejections (2/15 each; Fig. 1I and J). Strikingly, the combination of anti-CD39 and anti-PD-1 further slowed tumor growth and caused 7 out of 16 complete rejections (Fig. 1I and J).

Mechanism of Action of Anti-CD39 mAbs: Role of T Cells and IFN γ *In Vivo*

Given the single-agent antitumor efficacy of the anti-mouse CD39 antibody B66 in the MC38 tumor model, we used this model and a 200 μ g dose schedule to evaluate the mechanism of action of this mAb in subsequent experiments. In a broad first evaluation, we determined that anti-CD39 antitumor efficacy was completely host lymphocyte- and CD39-dependent (Fig. 2A). Dependence on host CD39 was confirmed in a second MCA1956 tumor model (Fig. 2B). Bone marrow chimeras of congenic wild-type (WT; *Ptprc*^a, *CD45.1*) and *Cd39*^{-/-} mice confirmed that anti-CD39 required hematopoietic CD39, but not nonhematopoietic CD39, for efficacy against MC38 tumors (Fig. 2C and D). Deeper

Figure 2. Mechanism of action of anti-CD39 mAb: role of T cells. **A**, Host lymphocyte- and CD39-dependent tumor growth control by anti-CD39 mAb. Groups ($n = 5$ –6/group) of WT, *Rag2*^{-/-} *γ c*^{-/-}, or *Cd39*^{-/-} mice were injected subcutaneously with MC38 (1×10^5) colon adenocarcinoma cells on day 0 and treated intraperitoneally with cIg (200 μ g) or anti-CD39 (200 μ g) on days 7, 10, 13, and 16. **B**, Anti-CD39 mAb efficacy against MCA1956 tumor growth is host CD39-dependent. Groups ($n = 10$ /group) of WT and *CD39*^{-/-} mice were injected subcutaneously with MCA1956 (1×10^6) fibrosarcoma cells on day 0 and treated intraperitoneally with cIg (200 μ g) or anti-CD39 (200 μ g) on days 10, 13, 16, and 19. **C** and **D**, Anti-CD39 mAb efficacy requires hematopoietic CD39. Groups ($n = 5$ /group) of WT (*Ptprc*^a) and *Cd39*^{-/-} bone marrow chimeric mice (generated 4 ways) were injected subcutaneously with MC38 (1×10^5) colon adenocarcinoma cells on day 0 and treated intraperitoneally with cIg (200 μ g) or anti-CD39 (200 μ g) on days 7, 10, 13, and 16. **E**, CD8⁺ T cell- and IFN γ -dependent MC38 tumor growth control by anti-CD39 mAb. Groups ($n = 7$ –10/group) of WT mice were injected subcutaneously with MC38 (1×10^5) colon adenocarcinoma cells on day 0 and treated intraperitoneally with either cIg (200 μ g) or anti-CD39 (200 μ g) on days 8, 11, 14, and 18 and cIg (100 μ g), anti-asGM1 (50 μ g), anti-CD8 β (100 μ g), or anti-mIFN γ (250 μ g) on days 7, 8, 14, and 21. Tumor sizes (mm²) were measured at the indicated time points and presented as mean \pm SEM. All experiments were performed once unless indicated. Significant differences among treatment groups were determined by a two-way ANOVA, followed by the Tukey multiple-comparisons test (*, $P < 0.05$; **, $P < 0.01$; ****, $P < 0.0001$). **F–I**, Groups ($n = 4$ –8/group) of WT mice were injected subcutaneously with MC38 (1×10^5 ; **F** and **G**) or MC38-OVA^{dim} (1×10^6 ; **H** and **I**) colon adenocarcinoma cells on day 0. Mice were treated intraperitoneally with cIg (200 μ g) or anti-CD39 (200 μ g) on day 7. Samples of tumor and spleen were collected 48 hours after mAb injection and processed for single-cell suspensions and then subjected to flow cytometry after *ex vivo* stimulation for 4 hours. **F** and **G**, Graphs showing frequencies of tumor-infiltrating CD8⁺ T cells expressing the indicated surface and intracellular molecules (mean \pm SEM with individual values). Data pooled from two experiments. **H**, Graphs showing frequencies of OVA-tetramer⁺ T cells as a proportion of total TCR β ⁺CD8⁺ T cells in the tumor and spleen. **I**, Graphs showing numbers of total OVA-tetramer⁺ T cells and those expressing IFN γ in the tumor and spleen. All experiments were performed once unless indicated. Significant differences between the indicated groups were determined by a two-way ANOVA, followed by Sidak multiple-comparisons test (**F**, **G**) or Mann-Whitney test (**H**; *, $P < 0.05$; **, $P < 0.01$; ****, $P < 0.0001$).



exploration by depleting CD8⁺ T cells or NK cells or neutralizing IFN γ revealed that anti-CD39 efficacy was CD8⁺ T cell- and IFN γ -dependent, but independent of NK cells (Fig. 2E). Additional analysis using mice defective in IFN γ (Supplementary Fig. S6A) or cytotoxic pathways (perforin, FasL) or neutralized for TRAIL (Supplementary Fig. S6B) or MC38 tumor cells overexpressing FLIP (to block all death receptor signaling; Supplementary Fig. S6C) demonstrated that anti-CD39 efficacy was dependent on IFN γ , but independent of the tested cytotoxic mechanisms.

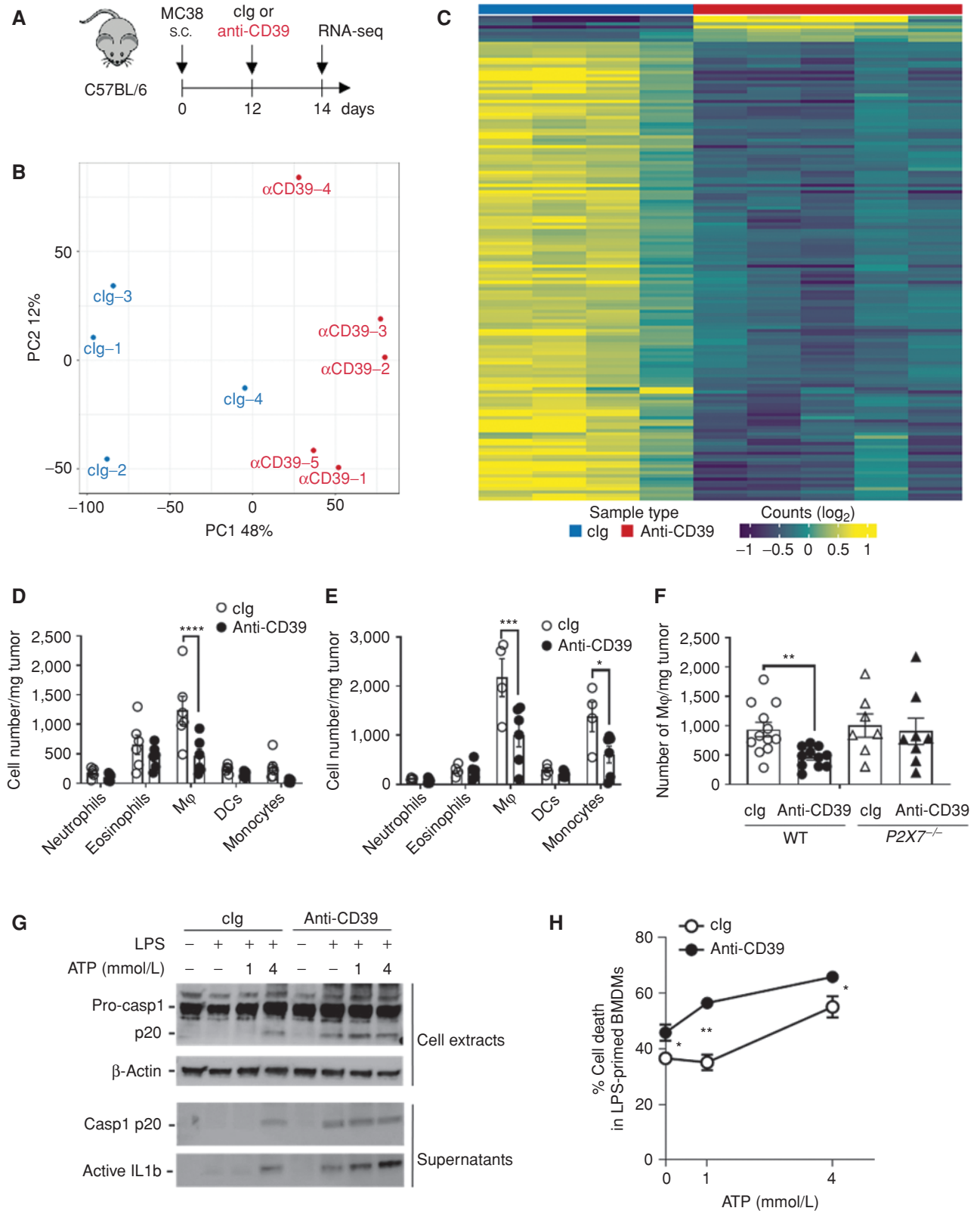
We next sought to examine various tumor and peripheral lymphoid organ immune cell subsets in the MC38 tumor model (gating shown in Supplementary Figs. S7 and S8A–S8E). Under anti-CD39 treatment conditions, within 48 hours the frequency of intratumor CD8⁺ T cells producing IFN γ , staining for Ki-67, and expressing PD-1 increased, and it was the CD39⁺ fraction of CD8⁺ T cells that increased in each case (Fig. 2F and G; Supplementary Fig. S8A and S8B). These changes occurred despite no obvious increase in CD45⁺ frequencies or subsets within them post anti-CD39 treatment at this early time point (Supplementary Fig. S8C). Similar changes in CD8⁺ T cells producing IFN γ , staining for Ki-67, and expressing PD-1 were not detected in the periphery (spleen and draining lymph node; Supplementary Fig. S8D). In the MC38-OVA^{dim} model, OVA-specific T cells were detected using tetramers 48 hours after anti-CD39 treatment. The percentage of OVA-tetramer⁺ T cells in tumor and spleen increased with anti-CD39 treatment; however, increases in the number of OVA-specific T cells and IFN γ ⁺ OVA-specific T cells were observed only in the tumors (Fig. 2H and I).

Mechanism of Action of Anti-CD39 mAb: Myeloid Changes *In Vivo*

To assess global changes mediated by targeting CD39, we performed RNA-sequencing (RNA-seq) analysis. MC38-bearing WT mice were treated with anti-CD39 (B66) or cIg, and whole-tumor tissues were harvested 48 hours later (Fig. 3A). Principal component and differential gene-expression analysis revealed significant changes induced by blocking CD39 in the TME (Fig. 3B and C; Supplementary Fig. S9A–S9C). Interestingly, the vast majority of the top 150 differentially expressed genes in Fig. 3C were downregulated in the anti-CD39 treatment group (Supplementary Table S1). Additionally, gene set enrichment analysis (GSEA) revealed that

anti-CD39 treatment induced a type I interferon response and led to the downregulation of gene signatures associated with immune suppression (Supplementary Fig. S9A and S9B). In line with our previous data, we observed downregulation of genes associated with immune-suppressive myeloid cells (39) in anti-CD39-treated tumors. We next sought to examine myeloid cell subsets in the MC38 tumor model on day 9 (48 hours after the first injection of cIg or anti-CD39; Fig. 3D) and day 15 (48 hours after the third injection; Fig. 3E). Under anti-CD39 treatment conditions, by day 9, the number of intratumor macrophages was reduced, and by day 15, both intratumor macrophages and monocytes were reduced. This reduction in intratumor macrophages did not occur in anti-CD39-treated *P2X7*^{-/-} mice compared with WT mice at day 9 (Fig. 3F). Other intratumor myeloid cell (DC) and granulocyte (eosinophils and neutrophils) subset numbers were equivalent in cIg- and anti-CD39-treated mice (Fig. 3D and E). Macrophage and monocyte depletion were also not detected in the spleen of these same treated mice (Supplementary Fig. S10). These data were consistent with anti-CD39-liberated eATP triggering macrophage pyroptosis (40), thus resulting in inflammasome activation with pro-caspase-1 cleavage, IL18/IL1 β release, and macrophage depletion. The death of lipopolysaccharide (LPS)-primed macrophages in the presence or absence of exogenously added ATP was greatly increased by anti-mouse CD39, and this was accompanied by pro-caspase-1 cleavage and release of active IL1 β (Fig. 3G and H). Collectively, these data possibly help explain the marked early decrease in myeloid genes as determined by whole-tumor RNA-seq analyses (Fig. 3C) and the reduction in intratumor macrophage number post anti-CD39 (Fig. 3D–F). Interestingly, anti-CD39 antitumor activity was also compromised following myeloid-cell depletion using clodronate liposomes or immobilization of myeloid-cell movement using anti-CD11b (Supplementary Fig. S11A). By contrast, additional experiments to deplete Ly6G⁺ neutrophils did not affect anti-CD39 antitumor activity (Supplementary Fig. S11B). These data highlight the likelihood that anti-CD39 antitumor activity is regulated by both intratumor macrophage pyroptosis and inflammasome activation. We also noted increased T-cell activation-related transcripts 48 hours after anti-CD39 treatment compared with cIg treatment, indicating stronger T-cell receptor (TCR) signaling (Supplementary Fig. S9C). Overall, our *in vivo*, flow-cytometry, and gene-expression data provide substantial

Figure 3. Flow cytometry and transcriptional signature analyses highlight macrophage reduction in tumors after anti-CD39 treatment. **A**, Schematic of experimental design. WT mice were injected subcutaneously with MC38 (1×10^5) colon adenocarcinoma cells on day 0. On day 12, mice were treated intraperitoneally with cIg or anti-CD39, and tumor samples were harvested 48 hours after treatment for RNA-seq. **B**, Principal component analysis of TMM normalized RNA-seq data for protein-coding genes from control samples (cIg, $n = 4$; colored blue) and treated samples (anti-CD39, $n = 5$; colored red). **C**, Heat map of top 150 differentially expressed genes between control (cIg) and treated (anti-CD39) samples. The gene-wise centered and scaled \log_2 values of TMM normalized counts are shown. The gene list is provided in Supplementary Table S1. **D** and **E**, Groups ($n = 4$ –6/group) of WT mice were injected subcutaneously with MC38 (1×10^5) colon adenocarcinoma cells on day 0 and treated intraperitoneally with cIg (200 μ g) or anti-CD39 (200 μ g) on days 7, 10, and 13. Tumor samples were collected on day 9 (**D**) and day 15 (**E**) and processed for single-cell suspensions and then subjected to flow cytometry. **D** and **E**, Summary bar graphs of numbers of MC38 tumor-infiltrating myeloid populations, as mean \pm SEM with individual values shown. Data represent one experiment (*, $P < 0.05$; ***, $P < 0.001$; ****, $P < 0.0001$, determined by a two-way ANOVA, followed by the Sidak multiple-comparisons test). **F**, Groups ($n = 7$ –12/group) of WT or *P2X7*^{-/-} mice were injected subcutaneously with MC38 (1×10^5) colon adenocarcinoma cells on day 0 and treated intraperitoneally with cIg (200 μ g) or anti-CD39 (200 μ g) on day 7. Tumor samples were collected on day 9 and processed for single-cell suspensions and then subjected to flow cytometry. **F**, Summary bar graphs of numbers MC38 tumor-infiltrating macrophages, as mean \pm SEM with individual values shown. Data are pooled from two experiments (**, $P < 0.01$, determined by the Mann-Whitney test). **G** and **H**, LPS-primed (100 ng/mL for 3 hours) bone marrow-derived macrophages (BMDM) were pretreated with cIg or anti-CD39 (10 μ g/mL), followed by stimulation with indicated concentrations of ATP for 90 minutes. **G**, Immunoblots showing indicated proteins from cell lysates and culture supernatants. **H**, Representative graphs showing the frequencies of propidium iodide-positive dead cells. Data, mean \pm SEM from triplicates from three experiments.



evidence that anti-CD39 reduces intratumor macrophage number and enhances intratumor T-cell activation.

Mechanism of Action of Anti-CD39 mAb: Critical Role of Myeloid CD39, P2X7, NALP3 Inflammasome, and IL18

Our data indicated that inhibition of CD39 enzymatic function led to an accumulation of eATP, which could lead to an activation of myeloid cells via P2X7. Therefore, we sought to examine expression of P2XY receptors on various tumor and peripheral lymphoid organ immune cell subsets in the MC38 tumor model on day 8 after tumor inoculation. A number of intratumor leukocyte populations expressed CD39 including a proportion (~25%–40%) of CD8⁺ T cells, FOXP3⁻ and FOXP3⁺ CD4⁺ T cells, and most of the innate NK cells, neutrophils, eosinophils, macrophages, DCs, and monocytes (Fig. 4A). CD73 was expressed on a greater fraction of T cells, but was generally lower in the proportions of innate leukocytes (Fig. 4B). However, P2X7 receptor expression was far more restricted. P2X7 and CD39 coexpression was notable only in 25% to 50% of macrophages and monocytes among all the aforementioned leukocytes (Fig. 4A and B). When looking outside the tumor (spleen and tumor-draining lymph node), CD39 expression was negligible in T cells, but still prevalent on innate leukocyte subsets (Supplementary Fig. S8E). P2X7 receptor was once again expressed by a proportion of macrophages and monocytes, but also by some DCs in the spleen and tumor-draining lymph node. To test the role of CD39 on myeloid cells, we created the LY2Z^{Cre/WT} CD39^{fl/fl} and LY2Z^{WT/WT} CD39^{fl/fl} strains of mice and examined anti-CD39 antitumor activity in the MC38 model (Fig. 4C). Anti-CD39 was inactive in global *Cd39*^{-/-} mice and conditional LY2Z^{Cre/WT} CD39^{fl/fl} mice, but active in WT mice and LY2Z^{WT/WT} CD39^{fl/fl} mice.

Positioned at the apex of the phosphohydrolytic cascade, CD39 is the pivotal regulator balancing proinflammatory eATP and immunosuppressive adenosine within the TME. P2X7 is the major functional eATP receptor on immune cells and is a critical factor in NALP3 inflammasome activity (41). Given this, we next examined whether host P2X7 receptor and downstream inflammasome components might be necessary for the antitumor activity of anti-CD39. MC38 tumors grew equivalently in WT, *Pycard*^{-/-}, and *Nalp3*^{-/-} mice, but more aggressively in *P2X7*^{-/-} mice. Importantly, anti-CD39 was effective against MC38 tumors in WT mice, but largely without activity in *P2X7*^{-/-}, *Pycard*^{-/-}, or *Nalp3*^{-/-} mice (Fig. 4D). Interestingly, anti-CD39 was ineffective in *P2X7*^{-/-} and *Nalp3*^{-/-} mice, but anti-PD-1 was effective in the same setting, suggesting a very different mechanism of action (Supplementary Fig. S12A). Anti-PD-1 and a combination of anti-PD-1 and A2AR were also equivalently effective in *Pycard*^{-/-} or *Nalp3*^{-/-} mice as WT mice (Supplementary Fig. S12B). The role of the inflammasome was further supported by the lack of antitumor activity of anti-CD39 in *Caspase-1*^{-/-}/*Caspase-11*^{-/-} mice (Fig. 4E).

The ability of anti-CD39 to trigger the inflammasome was supported by increased IL18 levels measured in MC38 tumor tissue lysates immediately post anti-CD39 therapy, in contrast to a lack of IL18 in similar tumors derived from *Nalp3*^{-/-} mice (Supplementary Fig. S13A). We next functionally tested the role of the inflammasome-generated IL1 β and

IL18, both of which have been shown to promote downstream T-cell antitumor function (42, 43). In both the MC38 and MCA1956 tumor models, blockade of IL18 over the course of anti-CD39 therapy completely abrogated the antitumor activity of anti-CD39 (Fig. 4F and G). Anti-IL1 β displayed partial blockade of anti-CD39 antitumor activity. These data were supported by additional experiments comparing cIg and anti-CD39 against MC38 and MCA1956 in WT versus *Il18*^{-/-} or *Il1r*^{-/-} mice (Supplementary Fig. S13B and S13C). Overall, we hypothesize that anti-CD39 may bind CD39 on P2X7-expressing intratumor macrophages and monocytes to liberate eATP, triggering the activation of the NALP3 inflammasome. The downstream activation release of IL18 and IL1 β and probably other factors then promote CD8⁺ T-cell proliferation and IFN γ -mediated effector function.

Anti-CD39 Turns “Cold” Anti-PD-1-Resistant Tumors “Hot” and Sensitive

One of the most pressing issues in cancer immunotherapy is that several tumor types show profound innate resistance to ICB, including anti-PD-1/anti-PD-L1 (2). Thus, we used the anti-CD39 and anti-PD-1 combination in a series of anti-PD-1-resistant and poorly T-cell infiltrated tumor models, including the BRAF-mutant melanoma SM1WT1, the MHC class I low melanoma B16F10, and the MHC class I low prostate carcinoma RM1 (Fig. 5). In each model, combined treatment displayed antitumor activity where either monotherapy was largely ineffective. Early treatment with anti-CD39 did have a minor impact in these models (Fig. 5A–C). Similar data were obtained with the anti-PD-1-refractory CT26 colon adenocarcinoma and HER2⁺ TUBO mammary cancers (Supplementary Fig. S14A and S14B). Consistent with our earlier report (44), in the latter setting, combinations of anti-PD-1 were very effective with anti-HER2, but so was the combination of anti-CD39 and anti-HER2 (Supplementary Fig. S14B). Assessment of anti-CD39 in the context of contemporary anti-PD-1 and anti-CTLA4 blockade in well-established B16F10 tumors again highlighted the additional benefit of anti-CD39 and its superiority to POM1 (Fig. 5D). Preliminary assessment of the mechanism of action of anti-PD-1 and anti-CD39 in the RM1 (Fig. 5E) and SM1WT1 (Supplementary Fig. S14C) tumor models revealed a CD8⁺ T cell- and IFN γ -dependent effect. The RM1 tumor model was interrogated in more depth, and a significant increase in the frequency of intratumor CD45⁺ cells, intratumor CD8⁺ T cells, and NK cells was detected 2 days after the third combination dose in the treatment schedule (day 14) where tumor mass had decreased (Fig. 5F and G; Supplementary Fig. S14D and S14E). CD8⁺ T-cell number per mg tumor mass was also increased in the combination-treated group (Supplementary Fig. S14F).

To corroborate our findings, we also used a model of adoptive cell transfer (ACT) immunotherapy to treat immune cell-poor melanoma (39). For this, WT mice were injected with HcMel12 melanoma expressing human gp100 under the control of the melanocytic lineage gene *Tyrp1*. Once tumors were established, mice were treated with our ACT protocol using gp100-specific pmel-1 TCR transgenic T cells (39, 45). Mice also received 5 doses of cIg or anti-CD39 (Supplementary Fig. S15A). The combination of ACT with anti-CD39 significantly inhibited tumor growth and improved survival (Supplementary Fig. S15B).

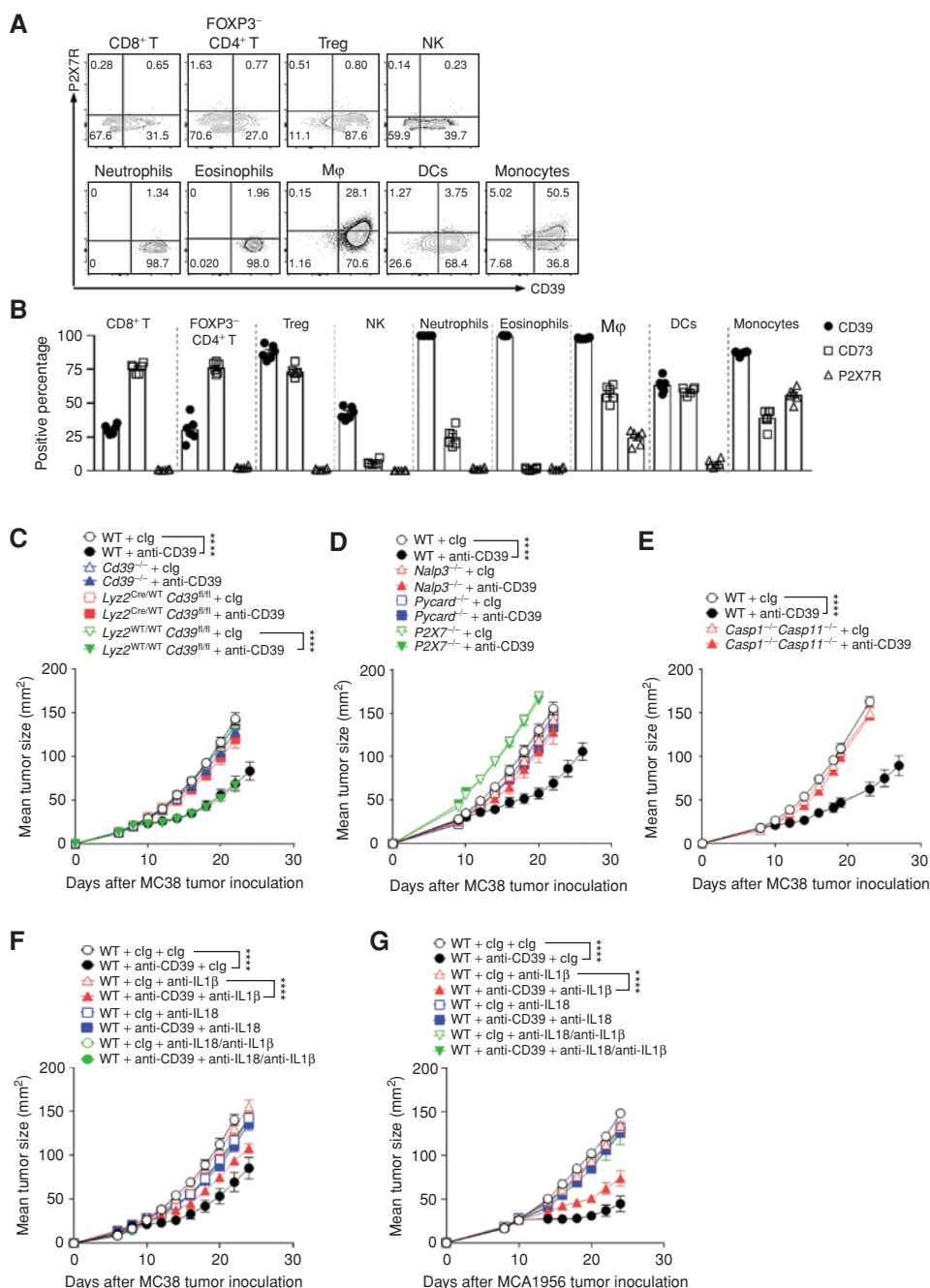


Figure 4. Mechanism of action of anti-CD39 mAb: role of myeloid cells, P2X7, and NALP3 inflammasome. **A** and **B**, Groups ($n = 4-8$ /group) of WT mice were injected subcutaneously with MC38 (1×10^5) colon adenocarcinoma cells on day 0. Samples of tumor and spleen were collected on day 8 and processed for single-cell suspensions and then subjected to flow cytometry. **A**, Representative FACS plots showing expression of CD39 and P2X7R on various tumor-infiltrating leukocytes (TIL) in MC38 tumors. **B**, Summary bar graphs of % CD39, CD73, and P2X7R expression on MC38 TIL subsets, as mean \pm SEM. **C**, Groups ($n = 6-7$ /group) of WT, *Cd39*^{-/-}, *Lyz2*^{Cre/WT} *Cd39*^{fl/fl}, and *Lyz2*^{WT/WT} *Cd39*^{fl/fl} mice were injected subcutaneously with MC38 (1×10^5) colon adenocarcinoma cells on day 0 and treated intraperitoneally with clg (200 μ g) or anti-CD39 (200 μ g) on days 8, 11, 14, and 17. **D**, Groups ($n = 5$ /group) of WT, *Cd39*^{-/-}, *Pycard*^{-/-}, and *Nalp3*^{-/-} mice were injected subcutaneously with MC38 (1×10^5) colon adenocarcinoma cells on day 0 and treated intraperitoneally with clg (200 μ g) or anti-CD39 (200 μ g) on days 9, 12, 15, and 18. **E**, Groups ($n = 6$ /group) of WT, and *Caspase1*^{-/-} *Caspase11*^{-/-} mice were injected subcutaneously with MC38 (1×10^5) colon adenocarcinoma cells on day 0 and treated intraperitoneally with clg (200 μ g) or anti-CD39 (200 μ g) on days 8, 11, 14, and 17. **C-E**, Representative of two experiments performed. **F**, Groups ($n = 5$ /group) of WT mice were injected subcutaneously with MC38 (1×10^5) colon adenocarcinoma cells on day 0 and treated intraperitoneally with clg (200 μ g) or anti-CD39 (200 μ g) on days 8, 11, 14, and 17. Mice additionally received intraperitoneally either clg (250 μ g), anti-IL1 β (250 μ g), anti-IL18 (250 μ g), or anti-IL1 β and anti-IL18 (250 μ g each) on days 7, 8, 15, and 22, respectively, after tumor inoculation. **G**, Groups ($n = 5$ /group) of WT mice were injected subcutaneously with MCA1956 (1×10^6) sarcoma cells on day 0 and treated intraperitoneally with clg (200 μ g) or anti-CD39 (200 μ g) on days 10, 13, 16, and 19. Mice additionally received intraperitoneally either clg (250 μ g), anti-IL1 β (250 μ g), anti-IL18 (250 μ g), or anti-IL1 β and anti-IL18 (250 μ g each) on days 9, 10, 17, and 24, respectively, after tumor inoculation. **C-G**, Tumor sizes (mm²) were measured at the indicated time points and presented as mean \pm SEM. All experiments were performed once unless indicated. Significant differences among treatment groups were determined by a two-way ANOVA, followed by the Tukey multiple-comparisons test (***) ($P < 0.0001$).

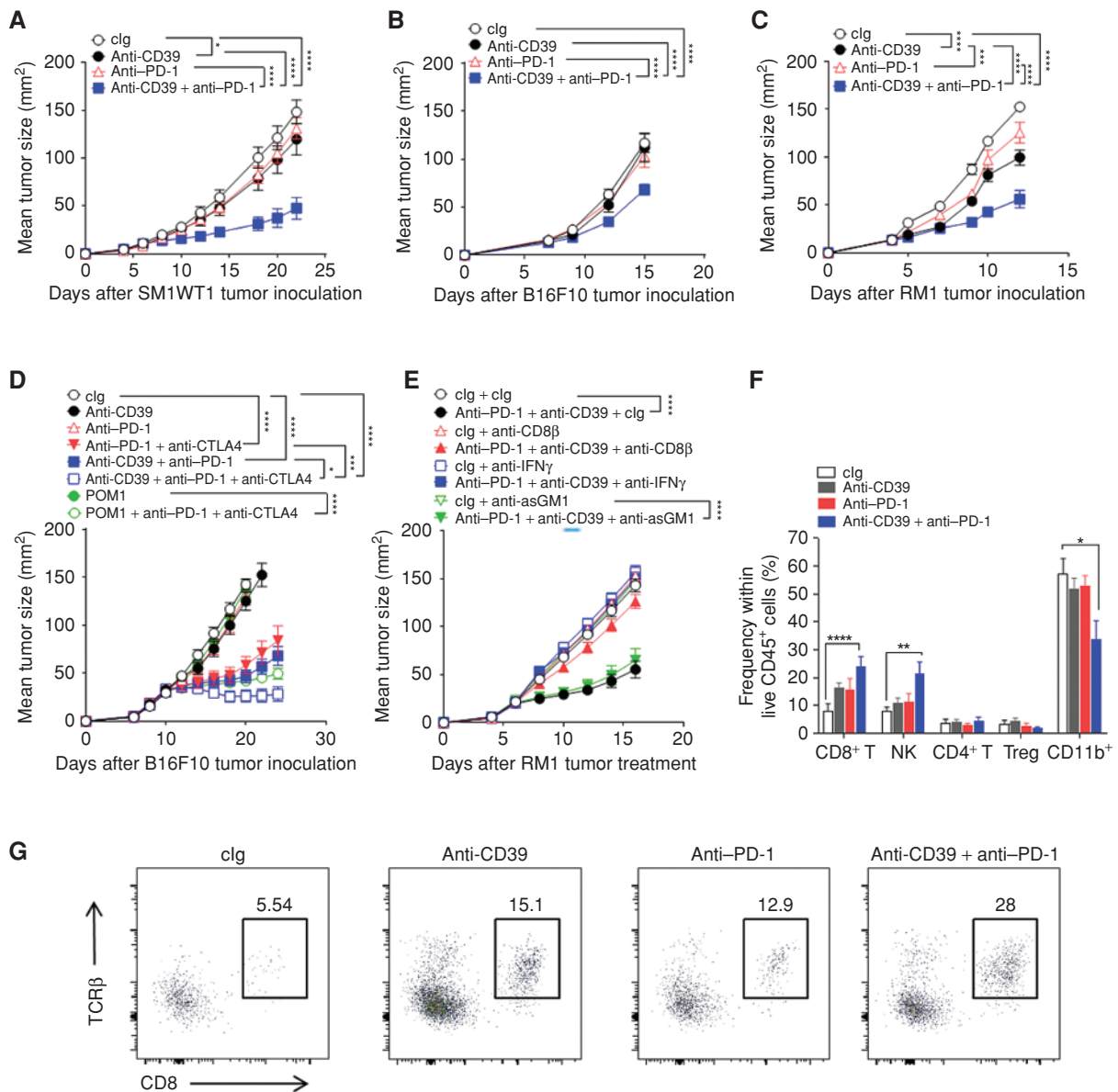


Figure 5. Anti-CD39 mAb sensitizes anti-PD-1-resistant tumors by increasing CD8⁺ T-cell infiltration. **A**, SM1WT1 tumors. Groups ($n = 6$ /group) of WT mice were injected subcutaneously with SM1WT1 melanoma cells (1×10^6) on day 0 and treated intraperitoneally with clg (200 μ g), anti-CD39 (200 μ g), anti-PD-1 (250 μ g), or anti-CD39/anti-PD-1 (200 μ g; 250 μ g) on days 6, 9, 12, and 14, respectively. **B**, B16F10 tumors. Groups ($n = 7$ –9/group) of WT mice were injected subcutaneously with B16F10 melanoma cells (1×10^5) on day 0 and treated intraperitoneally with clg (200 μ g), anti-CD39 (200 μ g), anti-PD-1 (250 μ g), anti-CD39/anti-PD-1 (200 μ g; 250 μ g) on days 7, 10, and 13. **C**, RM1 tumors. Groups ($n = 7$ –8/group) of WT mice were injected subcutaneously with RM1 prostate carcinoma cells (5×10^4) on day 0 and treated intraperitoneally with clg (200 μ g), anti-CD39 (200 μ g), anti-PD-1 (250 μ g), anti-CD39/anti-PD-1 (200 μ g; 250 μ g) on days 3, 6, 9, and 12, respectively. **D**, Combining anti-CD39, anti-PD-1, and anti-CTLA4 improves therapeutic efficacy in resistant B16F10 tumors. Groups ($n = 6$ –12/group) of WT mice were injected subcutaneously with B16F10 melanoma cells (1×10^5) on day 0 and treated intraperitoneally with clg (200 μ g), anti-CD39 (200 μ g), anti-PD-1 (250 μ g), anti-CTLA4 (250 μ g), or POM1 (250 μ g) alone or in various combinations as indicated on days 10, 13, 16, and 19, respectively. **E**, Combination efficacy is IFN γ - and CD8⁺ T-cell-dependent. Groups ($n = 6$ /group) of WT mice were injected subcutaneously with RM1 prostate carcinoma cells (5×10^4) on day 0 and treated intraperitoneally with clg (200 μ g), anti-CD39 (200 μ g), anti-PD-1 (250 μ g), or anti-CD39/anti-PD-1 (200 μ g; 250 μ g) on days 6, 9, 12, and 15. Some groups of mice were also treated intraperitoneally with either clg (100 μ g), anti-asGM1 (50 μ g), anti-CD8 β (100 μ g) or anti-mIFN γ (250 μ g) on days 5, 6, and 13, respectively. Tumor sizes (mm²) were measured at the indicated time points and presented as mean \pm SEM. Significant differences between the treatment groups were determined by a two-way ANOVA, followed by the Tukey multiple-comparisons test (*, $P < 0.05$; **, $P < 0.001$; ***, $P < 0.0001$). **F** and **G**, Groups ($n = 5$ –6/group) of WT mice were injected subcutaneously with RM1 prostate carcinoma cells (5×10^4) on day 0 and treated intraperitoneally with clg (200 μ g), anti-CD39 (200 μ g), anti-PD-1 (250 μ g), anti-CD39/anti-PD-1 (200 μ g; 250 μ g) on days 6, 9, and 12. The tumors were collected on day 14, 48 hours after the third dose, for TIL analysis by flow cytometry. **F**, Graphs showing the frequencies of immune cell subsets in RM1 tumors 2 days after the third injection of the indicated mAbs. **G**, Representative FACS plots showing increased CD8⁺ T-cell infiltration in RM1 tumors on day 14, 2 days after the third anti-CD39/anti-PD-1 mAb treatment. All experiments were performed once unless indicated. Significant differences in percentage between the selected cell populations were determined by one-way ANOVA, followed by the Tukey multiple-comparisons test (*, $P < 0.05$; **, $P < 0.01$; ***, $P < 0.0001$).

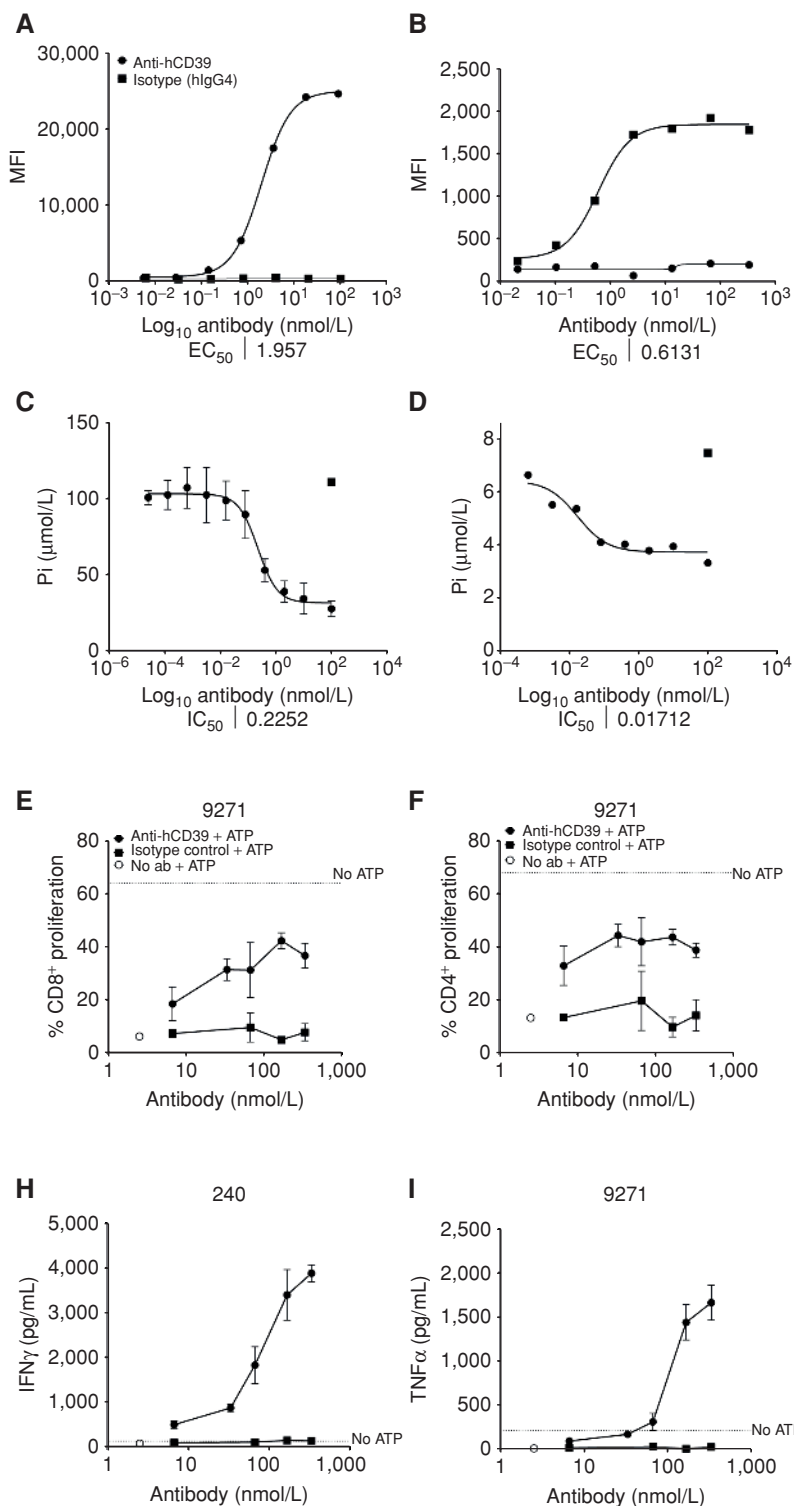


Figure 6. Human anti-CD39 mAb blocks CD39 enzymatic activity and enhances T-cell proliferation and effector function in the presence of ATP. **A–D**, Anti-hCD39 binds and inhibits CD39 enzymatic activity at subnanomolar potency. Anti-hCD39 mAb binds to the 721.221 cell line (**A**) and human monocytes (**B**) and inhibits CD39 enzymatic activity as measured by Pi release using the Malachite Green assay (**C** and **D**, respectively, and Supplementary Fig. 14). **E–J**, Anti-hCD39 enhances T-cell proliferation and Th1 cytokine production. Peripheral blood mononuclear cells (PBMC) from two different donors were stimulated with anti-CD3/anti-CD28 and either an isotype control or anti-human CD39, and assessed for T-cell proliferation in the presence and absence of ATP by flow cytometry. The graphs represent anti-hCD39-induced increased CD8⁺ (**E**) and CD4⁺ (**F**) T-cell proliferation in the presence of ATP (donor 9271), and increased IFNγ (**G** and **H**) and TNFα (**I** and **J**) production in PBMCs (donors 240 and 9271), treated with anti-hCD39 in the presence of ATP. Human IgG4 isotype control was used for comparison. MFI, mean fluorescence intensity.

Anti-Human CD39 mAb Increases T-cell Proliferation and Th1 Cytokine Secretion

The monotherapy and combination antitumor activity of B66, an anti-mouse CD39 mAb, was very encouraging, but it was critical to produce an anti-human CD39 for clinical

translation. Therefore, using yeast display of human V gene libraries, we produced a human IgG4 anti-human CD39 mAb, TTX-030 (46). This mAb bound human CD39 on 721.221 cells and human monocytes (Fig. 6A and B) and allosterically inhibited CD39 enzymatic activity on these cells (Fig. 6C and D; Supplementary Fig. S16A and S16B) at subnanomolar levels.

Functional assessment of anti-human CD39 *in vitro* in anti-CD3/anti-CD28-stimulated peripheral blood mononuclear cells (PBMC) from various donors demonstrated the potent ability of this mAb to enhance CD4⁺ and CD8⁺ T-cell proliferation (Fig. 6E and F; Supplementary Fig. S17A and S17B). Anti-human CD39 also increased Th1 cytokine production (IFN γ , TNF α , and IL2) in these cultures compared with a hIgG4 control mAb (Fig. 6G–J; Supplementary Fig. S17C–S17G).

Anti-Human CD39 mAb Activity with Autologous EBV-Specific Human T Cells

In the absence of having a fully humanized mouse model of cancer, we next decided to examine the antitumor activity of anti-human CD39 alone or in combination with autologous Epstein–Barr virus (EBV)-specific T-cell transfer against lymphoblastoid cell lines (LCL; EBV-transformed B cells) derived from the same donors inoculated into immunodeficient NRG mice. These mice lack all lymphocytes, and the only human CD39-expressing cells are the T cells and LCLs injected. All LCLs generated were highly CD39⁺ (Supplementary Fig. S18A), but we first selected donors based on the ability of their LCLs to grow robustly in NRG mice. Two donors were chosen (LCL039 and LC043), and preliminary experiments with these CD39⁺ LCLs and the CD39⁺ SK-MEL28 melanoma suggested that these were not sensitive to delayed anti-human CD39 treatment alone (Supplementary Fig. S18B and S18C).

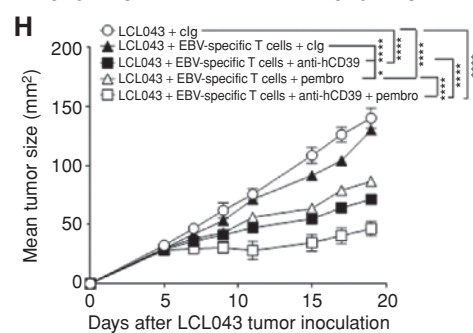
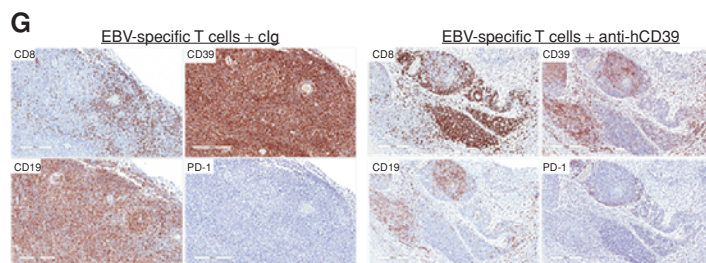
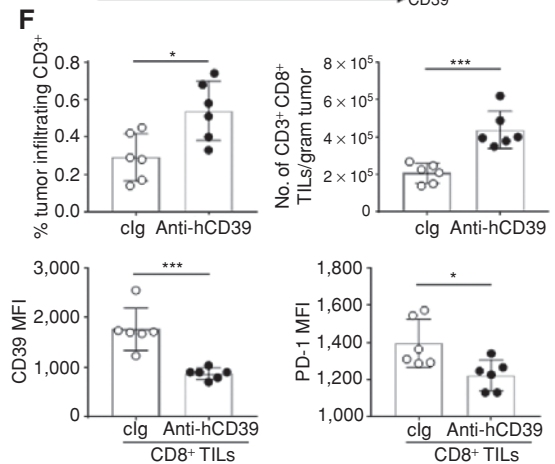
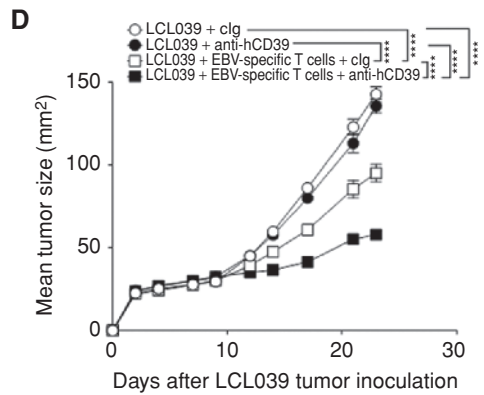
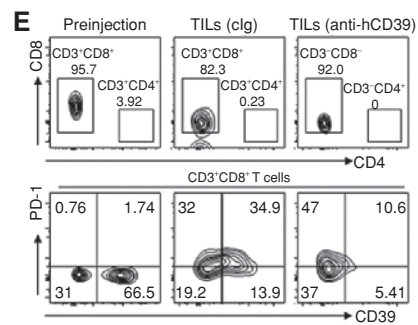
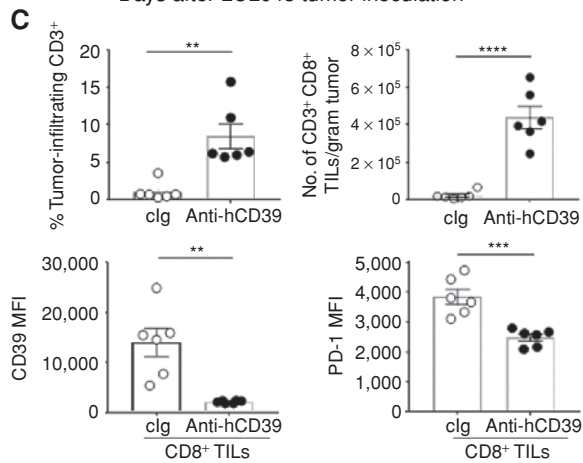
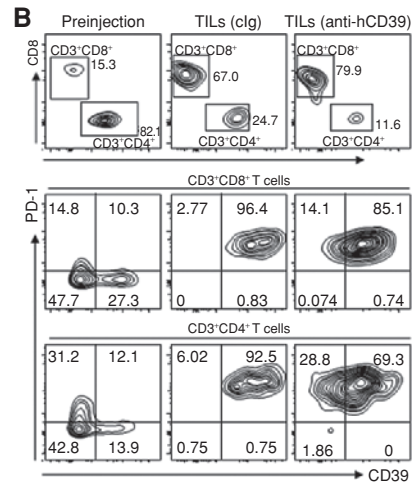
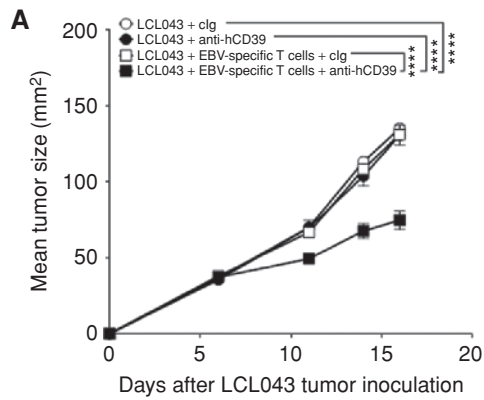
EBV-stimulated T-cell cultures from different donors are distinct, and those raised against LCL043 and LCL039 offered the opportunity to examine a mixed but predominantly CD4⁺ T-cell culture with significant CD39 and PD-1 coexpression on T cells (LCL043), and a predominantly CD8⁺ T-cell culture with a high proportion of CD8⁺ T cells expressing CD39, but largely lacking PD-1 expression (LCL039). In the case of LCL043, either EBV-specific T cells alone or anti-CD39 did not suppress tumor growth compared with cIg, but the combination of T cells and anti-CD39 did significantly

suppress tumor growth (Fig. 7A). Analysis of EBV-specific T cells preinjection and in the LCL043 lymphoma after injection (at endpoint day 17) revealed a significant increase in the CD8⁺:CD4⁺ T-cell ratio in the tumor regardless of whether cIg or anti-human CD39 was administered (Fig. 7B). Notably, however, anti-human CD39 increased the percentage of tumor-infiltrating CD3⁺ cells and the number of tumor-infiltrating CD3⁺CD8⁺ T cells compared with cIg-treated mice (Fig. 7C). Anti-human CD39 therapy also dramatically decreased the CD39 expression levels on intratumor CD8⁺ T cells compared with cIg treatment (Fig. 7C). A more modest reduction in PD-1 expression was also noted.

The LCL039 lymphoma had a lower tumorigenicity in NRG mice (than LCL043), but once again anti-CD39 alone was without effect. However, autologous EBV-specific T cells were more active alone in this setting (Fig. 7D) and again, following transfer, CD8⁺ T cells were enriched in the LCL tumor at endpoint (day 23; Fig. 7E and F). Consistent with the LCL043 experiments, anti-human CD39 enhanced the antitumor activity of autologous EBV-specific T cells (Fig. 7D) and increased the percentage of tumor-infiltrating CD3⁺ cells and the number of tumor-infiltrating CD3⁺CD8⁺ T cells compared with cIg-treated mice (Fig. 7F and G). Anti-human CD39 therapy again decreased the CD39 expression levels on intratumor CD8⁺ T cells compared with cIg treatment (Fig. 7F and G). PD-1 expression was increased on the CD8⁺ T cells after injection, and again anti-CD39 therapy appeared to reduce the expression levels of PD-1 on intratumor CD8⁺ T cells compared with cIg treatment (Fig. 7E and F).

Given the lack of effect of autologous EBV-specific T-cell transfer against established LCL043, and the limited antitumor activity of the anti-CD39 and T-cell combination, we performed a second experiment to evaluate the addition of pembrolizumab (anti-human PD-1). Here, anti-CD39 and anti-PD-1 displayed very similar antitumor activities when each was administered with autologous EBV-specific T cells, but demonstrated an even greater effect on tumor growth when combined together with T-cell transfer (Fig. 7H). In summary,

Figure 7. Anti-hCD39 mAb and EBV-specific T cells effectively control LCL tumor growth in NRG mice. **A**, Groups ($n = 6/\text{group}$) of NRG mice were injected subcutaneously with EBV-transformed lymphoblastoid cells LCL043 (1×10^7) on day 0. In some groups, EBV-specific T cells (9×10^6) were administered intravenously on day 5 as indicated, and all experimental groups were then treated intraperitoneally with either human cIg (250 μg) or anti-hCD39 (250 μg) on days 5, 8, 11, and 14. Tumor sizes (mm^2) were measured at the indicated time points and presented as mean \pm SEM. This experiment is representative of two performed. Significant differences between the indicated groups were determined by a two-way ANOVA, followed by Tukey multiple-comparisons test (****, $P < 0.0001$). **B** and **C**, From **A**, tumors were collected, and single-cell suspensions were made and subjected to flow cytometry. **B**, Representative FACS plots of preinjection EBV-specific T-cell cultures and tumors post cIg or anti-CD39 (TTX-030) therapy (day 17 after tumor inoculation) and summary bar graphs showing frequencies of tumor-infiltrating CD3⁺ T cells, numbers of CD3⁺CD8⁺ T cells, and expression levels of CD39 and PD-1 on CD8⁺ T cells in LCL tumors post cIg or anti-CD39 therapy (**C**). Significant differences were determined by the Mann–Whitney U test (**, $P < 0.01$; ***, $P < 0.001$; ****, $P < 0.0001$). **D**, Groups ($n = 6/\text{group}$) of NRG mice were injected subcutaneously with donor-derived EBV-transformed lymphoblastoid cells LCL039 (1×10^7) on day 0. In some groups, EBV-specific T cells (9×10^6) were administered intravenously on day 10 as indicated, and all experimental groups were then treated intraperitoneally with anti-hCD39 (250 μg) or human cIg (250 μg) on days 10, 13, 16, and 19. Tumor sizes (mm^2) were measured at the indicated time points and presented as mean \pm SEM. This experiment is representative of two performed. Significant differences between the indicated groups were determined by a two-way ANOVA, followed by the Tukey multiple-comparisons test (****, $P < 0.0001$). **E** and **F**, From **D**, tumors were collected, and single-cell suspensions were made and subjected to flow cytometry. **E**, Representative FACS plots of preinjection EBV-specific T-cell cultures and tumors post cIg or anti-human CD39 therapy (day 23 after tumor inoculation) and summary bar graphs showing frequencies of tumor-infiltrating CD3⁺ T cells, numbers of CD3⁺CD8⁺ T cells, and expression levels of CD39 and PD-1 on CD8⁺ T cells in LCL tumors post cIg or anti-CD39 therapy (**F**). Significant differences in percentages between the selected cell populations were determined by the Mann–Whitney test (*, $P < 0.05$; ***, $P < 0.001$). **G**, Representative IHC staining of CD8, CD39, PD-1, and CD19 on day 23 (endpoint) LCL039 tumors showing increased CD8⁺ T-cell infiltration and reduced CD39 expression in the EBV-specific T-cell/anti-hCD39-treated tumors. **H**, Anti-hCD39 and pembrolizumab combine with autologous EBV-specific T cells to suppress human B-cell LCL043 lymphoma. Groups ($n = 6/\text{group}$) of NRG mice were injected subcutaneously with EBV-transformed lymphoblastoid cells LCL043 (1×10^7) on day 0. In some groups, EBV-specific T cells (9×10^6) were administered intravenously on day 5 as indicated, and all experimental groups were then treated intraperitoneally with human cIg (250 μg) or anti-hCD39 (250 μg) or pembrolizumab (anti-human PD-1; 250 μg) or both (250 μg ; 250 μg) on days 5, 8, 11, and 14. Tumor sizes (mm^2) were measured at the indicated time points and presented as mean \pm SEM. All experiments were performed once unless indicated. Significant differences between the indicated groups were determined by a two-way ANOVA, followed by Tukey multiple-comparisons test (*, $P < 0.05$; ***, $P < 0.001$; ****, $P < 0.0001$).



the anti-human CD39 antibody enriches intratumor human CD8⁺ T-cell number and suppresses human B-cell lymphoma following autologous EBV-specific T-cell transfer.

DISCUSSION

This study is the first to describe an mAb specifically targeting mouse CD39, and as such we have been able to undertake comprehensive mechanism-of-action experiments in immunocompetent and gene-targeted mice. All prior assumptions regarding CD39 have been based on studies using small-molecule inhibitors of CD39 (31), *Cd39*^{-/-} mice (30), and other genetic strategies to target CD39 (47) or anti-human CD39 mAbs *in vitro* or in immune-compromised mice (17, 32). The previous approaches have limitations with respect to translation and are inferior to assessing a potent anti-mouse CD39 mAb in syngeneic tumor models. Furthermore, our study has uncovered the critical importance of an eATP-P2X7-ASC-NALP3-inflammasome-IL18 pathway in the antitumor activity mediated by CD39 enzyme blockade. This pathway has not previously been recognized to be critical for anti-CD39 antitumor activity. Rather, previous experimental evidence supported a dogma where blockade of CD39 primarily prevented CD73 from generating adenosine as a mechanism of action. eATP liberation and signaling of immune stimulation has been postulated as a mechanism of action of CD39 blockade, but this has never been demonstrated with any experimental evidence. Our data suggest that anti-CD39 activity is mediated by CD39 and P2X7 coexpression on intratumor myeloid-cell subsets, an early signature of macrophage depletion, and active IL18 release that facilitates subsequent T-cell effector function. In syngeneic mice and autologous human T cell-tumor models, anti-CD39 effectively converted T cell-poor tumors into T cell-rich tumors and rescued anti-PD-1 resistance.

Despite the impressive advances achieved by immunotherapies in the past few years, there is a significant proportion of patients whose cancer is refractory to ICB or who develop adaptive resistance after achieving initial clinical responses. In either case, there is a growing body of evidence to suggest that adenosine-mediated immunosuppression is a major mechanism of immune evasion underlying these observations (48–50). These insights are supported by the increasing evidence gleaned from extensive immunophenotyping efforts. Dissection of the TME via flow cytometry, CyTOF, IHC, or single-cell RNA-seq analysis have revealed that upregulation of CD39 expression on critical tumor-infiltrating immune subsets is a common occurrence across multiple tumor types (23, 24, 51). The presence of high levels of CD39 on regulatory immune subsets (18–21) and on exhausted and tumor-reactive T cells (23–25) is directly correlated with immune dysfunction. Meanwhile, CD39 expression on the tumor itself appears to be restricted to a small subset of patients in most indications (32) or specific indications where increased prevalence has been reported (e.g., blood malignancies or melanoma; ref. 52). Given these observations, our finding that inhibiting CD39 expression on the myeloid compartment is required for reversing immune suppression within the TME has implications for patients with cancer who may benefit from anti-CD39 therapy.

First, although patients with immunologically active, “hot” tumors are more likely to respond to existing immune-checkpoint inhibitors, the majority still fail to achieve complete, durable responses. If adenosine-mediated immune suppression is indeed a major source of this innate or adaptive resistance, then disruption of the adenosinergic pathway might be effective in settings where immune infiltrates are present but either immune-checkpoint inhibitors fail to elicit antitumor responses or patients relapse as adaptive resistance develops. Second, we have demonstrated that inhibition of CD39 enzymatic function can sensitize intrinsically resistant, “cold” tumor models to anti-PD-1. Given that ICB has generally failed in settings where the preexisting TME is T-cell poor, this potentially opens up new indications for consideration. Our findings both in a poorly infiltrated syngeneic tumor model and in the humanized setting indicate that blocking CD39 enzymatic activity is correlated with the increased infiltration of cytotoxic effector populations into the TME and a concomitant upregulation of activation markers on those infiltrates. Although eATP has been reported as a chemotactic signal for attracting myeloid populations, especially neutrophils via P2Y2 (53, 54), we see a decrease in intratumor macrophages.

One potential explanation is offered by the observation that activation of the inflammasome appears necessary to achieve the full therapeutic benefit of CD39 enzymatic inhibition. In the context of the broader therapeutic landscape, this impact on innate immune function and antigen-presenting subsets may be a key feature that distinguishes CD39 enzymatic inhibition from other modalities targeting the adenosinergic axis. Indeed, the NALP3 inflammasome was not required for the antitumor activity of anti-PD-1 or anti-PD-1 and A2ARi. In direct comparisons of antitumor activity, inhibition of CD39 enzymatic function was superior to antagonism of CD73 enzymatic function and/or downstream A2AR/A2BR signaling. Unlike therapeutic approaches that target the downstream production or function of adenosine, inhibition of CD39 not only limits the production of adenosine but also prevents the rapid degradation of eATP in the TME. eATP is therefore made available to trigger purinergic receptors on both innate and adaptive immune cells (55, 56). Also interesting was the finding that anti-CD39 was able to further suppress tumor immunity in mice blocked or deleted for CD73, A2AR, and A2BR. This suggests that not all extracellular adenosine was inhibited by anti-CD39 and perhaps other adenosine-generating pathways may contribute when CD39 is blocked. Whether similar combination effects can be achieved by locally inhibiting HIF1/hypoxia as a major regulator of CD39 and CD73 remains to be determined (57). These data also confirm the distinct mechanism of action of anti-CD39. Further delineation of the adaptive versus innate contributions of eATP will require conditional P2X7 gene-targeted mice to dissect the relative contributions of immune subsets, but is warranted in light of these findings.

Surprisingly, global CD39 gene-targeted mice often did not display a tumor reduction phenotype where the anti-CD39 mAb treatment was very effective. This suggests either compensation in the CD39 gene-targeted strain involving other molecules (e.g., CD38) or different protumor and antitumor roles of CD39 when expressed on different cell types. LY22^{Cre/WT} CD39^{fl/fl} mice did not display any profound tumor-resistance phenotype, but clearly did not respond

upon anti-CD39 treatment. LY2Z^{Cre/WT} CD39^{fl/fl} mice display a decrease in macrophage, monocyte, and neutrophil CD39 expression, but only macrophages and monocytes are reduced in tumors post anti-CD39 treatment and only these myeloid cells coexpress CD39 and P2X7 in the TME. Thus, it seems likely that intratumor myeloid cells expressing CD39 coexpress P2X7 and respond to the eATP liberated by anti-CD39. This response includes NALP3 inflammasome activation, IL18/IL1 β release, and pyroptosis. Consistent with this mechanism, depletion or immobilization of myeloid cells or neutralization of IL18/IL1 β completely abrogated the anti-tumor activity of anti-mouse CD39. It remains to be determined whether this mechanism of action applies in “cold” mouse tumors and human tumors. “Hot” and “cold” mouse tumors all have some level of immunosuppressive myeloid cells expressing CD39, but it is clearly more difficult to determine mechanism of action in “cold” tumors where anti-CD39 monotherapy is weak. Macrophages and monocytes were reduced in both “hot” MC38 (Fig. 3D) and “cold” RM1 tumors 48 hours after anti-CD39 (Supplementary Fig. S19). Interestingly, in the EBV-specific T cell-LCL model, anti-human CD39 was effective only against established tumors when T cells were transferred despite the fact that the only human components were the human T cells and the human B-cell lymphoma expressing CD39. Here, it is possible that the transferred T cells or LCL tumors are the primary target of anti-human CD39. It is possible that LCLs may act as antigen-presenting cells in the autologous model and provide a source of IL18, and hence in this setting the need for myeloid cells might be bypassed. The contribution of mouse myeloid cells in this model has also not been assessed. Further experiments deleting CD39 in tumors and T cells will be required in mouse and humanized mouse tumor models to understand the importance of CD39 on these cells.

Our findings reveal insight into the effects of pharmacologic inhibition of CD39 enzymatic activity on the TME. Previously, this has mostly been studied in the context of genetic deletion of CD39 in the host (28, 30, 31, 58). Although these studies provide valuable insights into the role of the adenosinergic system in cancer, genetic knockout can be subject to compensatory mechanisms, including desensitization of the purinergic receptors (59). POM1 has also been used in mouse models to probe the importance of CD39 enzymatic function in cancer settings (28, 31, 51), but these studies are inherently limited by the lack of drug-like properties of this compound, including its poor serum half-life and broad ectonucleotidase specificity. Our studies suggest that enzymatic inhibition of CD39 by an antibody is in fact superior to both genetic deletion and POM1-mediated inhibition. This is also true in metastatic models where NK cells are effectors (manuscript in preparation). Antibody binding of CD39 without enzyme inhibition was not effective. The ability of anti-CD39 to inhibit CD39 ATPase activity was demonstrated *in vivo* and suggests a potential biomarker strategy for efficacy in humans should fresh-frozen tumor tissue be available.

In summary, our findings present compelling evidence for the impact of enzymatic inhibition of CD39 on the course of tumor progression. Translation of these preclinical findings into human trials will ultimately be required to determine the utility of this approach to treating human cancers, either as a

monotherapy or in combination with other established or to-be-discovered agents. First-in-human trials of the anti-CD39 in patients with advanced cancer have recently commenced (NCT03884556).

METHODS

Mice

WT C57BL/6 and BALB/c mice were purchased from the Walter and Eliza Hall Institute for Medical Research or bred in house. C57BL/6 *Ptprca* (CD45.1⁺) mice, C57BL/6 CD39-deficient (*Cd39*^{-/-}) mice (60), C57BL/6 NALP3-deficient (*Nalp3*^{-/-}) mice, C57BL/6 P2X7-deficient (*P2X7*^{-/-}) mice (61), C57BL/6 ASC-deficient (*Pycard*^{-/-}) mice, and NOD-RAG1-gamma c (NRG) mice were bred in house and maintained at the QIMR Berghofer Medical Research Institute. C57BL/6 *Rag2*^{-/-} γ c^{-/-} mice have been previously described (33). C57BL/6 LY2Z^{Cre/WT} CD39^{fl/fl} and LY2Z^{WT/WT} CD39^{fl/fl} mice were generated by crossing LY2Z^{Cre} mice (from Dr. Irmgard Foerster, University of Dusseldorf; ref. 62) with CD39^{fl/fl} mice (obtained from the EUCOMM Consortium). Mice greater than 6 weeks of age were sex-matched to the appropriate models. The number of mice in each group treatment or strain of mice for each experiment is indicated in the figure legends. In all studies, no mice were excluded based on preestablished criteria, and randomization was applied only immediately pretreatment in therapy experiments to ensure similar mean tumor size was the starting point. Experiments were conducted as approved by the QIMR Berghofer Medical Research Institute Animal Ethics Committee.

Human Ethics

Healthy volunteers under written informed consent were recruited according to the principles of the Declaration of Helsinki and the National Statement on Ethical Conduct in Human Research in accordance with the National Health and Medical Research Council (Australia) Act. The Human Ethics Committee of QIMR Berghofer Medical Research Institute approved the protocol for the recruitment of healthy volunteers. PBMCs from healthy volunteers were isolated using Ficoll–Paque gradients on SepMate columns (STEMCELL Technologies) and used to generate EBV-transformed LCLs as described previously (63). Autologous LCLs were used to generate EBV-specific T cells as outlined below. Alternatively, human PBMCs were isolated from a human peripheral blood leukopak purchased from STEMCELL Technologies. Using Institutional Review Board-approved consent forms and protocols, the material was obtained and distributed by STEMCELL for the purpose of *in vitro* research only.

Antibody Generation

The B66 antibody to murine CD39 was discovered through immunization of WT Sprague Dawley rats followed by hybridoma screening. Hits were produced as antibodies with Fc region derived from mouse IgG1 and were confirmed for binding to recombinant mCD39 extracellular domain (R&D Systems, cat. #4398-EN) or to mouse cells endogenously expressing CD39: BCL1, clone 5B1b (ATCC, cat. #TIB-197). The D265A variant was generated using QuikChange site-directed mutagenesis (Agilent). Anti-human CD39 (TTX-030) was previously generated via phage display with a human Fab library and expressed by standard techniques (46).

Anti-CD39 Efficacy In Vitro: Proliferation and Cytokine Effector Function

PBMCs were labeled with CellTrace Violet (Thermo Fisher) to measure proliferation, and 50,000 cells per well were plated into a 96-well round-bottom plate. Cells were pretreated for 30 minutes with antibody in triplicates, then 2 μ L Immunocult human CD3/CD28 T-cell activator (STEMCELL) was added per well in addition to

50 $\mu\text{mol/L}$ final concentration of ATP or medium alone (no ATP control). Cells were incubated for 96 hours, then spun at 1,700 rpm for 2 minutes. Supernatants were collected for evaluation of cytokines using Meso Scale Discovery. For flow cytometry, Human BD Fc Block was added to cells for 30 minutes before staining with CD4-PE/Cy7 (clone RPA-T4), CD8-APC (clone RPA-T8), CD3-Brilliant Violet 785 (BV785, clone OKT3), CD14-Alexa Fluor 488 (clone HCD14), and eBioscience Fixable Viability dye eFluor 780 (e780) for 30 minutes. Cells were washed twice and then resuspended in staining buffer and run on BD Fortessa. Data were analyzed on FlowJo, and CD4⁺ and CD8⁺ T-cell proliferation was plotted as a histogram. Unstimulated cells were used to set a control peak for nondividing cells, and the remaining peaks were analyzed as a percentage of proliferation.

Cell Culture

Mouse B16F10 (melanoma), MC38 (colon adenocarcinoma), and RM1 (prostate carcinoma) cells were grown in Dulbecco's Modified Eagle Medium supplemented with 10% fetal calf serum (Bovogen), 1% glutamine (Gibco), 1% HEPES (Gibco), and 1% penicillin/streptomycin (Gibco). Mouse SM1WT1 (melanoma), MCA1956 (fibrosarcoma), and 4T1.2 (mammary carcinoma) cells were cultured in RPMI-1640, supplemented with 10% fetal calf serum (Bovogen), 1% glutamine (Gibco), and 1% penicillin-streptomycin (Gibco; complete RPMI). All the mouse tumors were CD39 negative in culture as previously demonstrated (31). Human EBV-transformed lymphoblastoid cell lines (LCL039 and LCL043) were established from healthy seropositive donors as previously described (64) and were routinely maintained in complete RPMI. Mouse bone marrow-derived macrophages were generated in complete RPMI supplemented with M-CSF (20 ng/mL, PeproTech) for 6 days. All cell lines were maintained at 37°C, 5% CO₂, except MC38, which was cultured at 10% CO₂. Cell-injection and monitoring procedures were described in previous studies (64). All cell lines were routinely tested negative for *Mycoplasma*, but cell line authentication was not routinely performed.

Bone Marrow Chimera Construction

As previously described, CD45.1⁺*Ptprc*^a WT mice and CD45.2⁺*Cd39*^{-/-} mice as recipient mice (9–10 mice per group) were irradiated twice with a total dose of 1,050 cGy (33). Donor BM cells (1×10^7) from *Ptprc*^a mice or *Cd39*^{-/-} mice were then i.v. injected into the irradiated mice to construct the BM chimeric mice. Neomycin-containing water (1 mg/mL) was given to these mice for 3 weeks. After confirming the BM reconstruction by flow cytometry of peripheral blood 8 weeks after BM cell injection, MC38 cells (1×10^5) were subcutaneously injected into the BM chimeric mice. Mice were then treated intraperitoneally (i.p.) with cIg or anti-CD39 mAb as indicated, and tumor size was measured at the time points indicated in the figure legends.

Subcutaneous Tumor Models

For primary tumor growth experiments, MC38 (1×10^5), B16F10 (1×10^5), MCA1956 (1×10^6), RM1 (5×10^4), or SM1WT1 (1×10^6) cells were subcutaneously injected into mice in a final volume of 100 to 200 μL (day 0). Therapeutic antibody treatment commenced as indicated on days 3 to 10 after tumor inoculation and was given every 3 or 4 days up to a maximum of 4 doses. Digital calipers were used to measure the perpendicular diameters of the tumors. The tumor size was calculated and is presented as mean \pm SEM.

MCA-Induced Fibrosarcoma

Groups of 10 to 16 male C57BL/6 WT mice were inoculated subcutaneously in the hind flank with 300 μg of MCA (Sigma-Aldrich) in 0.1 mL of corn oil. Mice were treated with mIgG1, anti-CD39 (B66), anti-PD-1 (RMP1-14), or their combination (100 μg each, i.p., twice/week) for 6 weeks from the second palpable tumor measurement

(0.1–0.4 cm², days 77–127 relative to MCA inoculation). Mice were then monitored for fibrosarcoma development for 250 days with measurements made with a caliper as the product of two perpendicular diameters (cm²). The number of mice that rejected tumors out of the total number of mice is shown. Growth rate of tumor was also measured from treatment start point to sacrifice or tumor rejection (as mm²/day).

Generation of CTL Using LCL

To generate cytotoxic T lymphocytes (CTL) that predominantly recognize the immunodominant latent antigens of EBV (EBNA3-6), PBMCs were prepared prior to use and stored in liquid nitrogen. To prepare stimulator cells, 1×10^6 to 2×10^6 autologous LCLs were harvested and γ -irradiated at 80 Gy. PBMCs were resuspended and cultured with stimulator cells in a final ratio of 30:1, with IL2 in the medium (120 IU/mL). Additional IL2 and medium were added every 3 to 4 days until the end of the culture period. On day 21, cells were removed from the incubator, and the number of viable cells was determined using the Trypan blue exclusion method. The expanded CTLs were stored for further experiments.

Adoptive Transfer of EBV-Specific T Cells

NRG mice were grafted subcutaneously with 10^7 EBV-transformed lymphoblastoid cells (LCL039 or LCL043) per mouse. Tumor growth was monitored every 2 to 3 days using digital calipers. Five days (LCL043) or 10 days (LCL039) after engraftment of lymphoblastoid cells, mice were either mock-treated or infused with 9×10^6 EBV-specific T cells. Control Ig (palivizumab hG4; MedImmune) or anti-human CD39 (Tizona) were administered i.p. on the same day of EBV-specific T-cell injection and every 3 days for 4 doses in total. At the endpoint, tumors were resected and either digested with a combination of collagenase type 4 (Worthington Biochemical Corp.) and DNase I (Roche) at 37°C or fixed with formalin. Tumor-infiltrating CD8⁺ lymphocytes and expression of exhaustion markers were detected by flow cytometry and IHC.

In Vivo Treatments

For mouse tumor models, some groups of mice received either anti-CD8 β (53.5.8; BioXCell) as indicated to deplete CD8⁺ T cells or anti-asialoGM1 (Wako) to deplete NK cells. Some groups of mice were neutralized for IFN γ (H22) using the scheduling and dosing as indicated. Some mice were treated with cIg (I-1 or I-536, Leinco), anti-mouse CD39 (B66, mIgG1, Tizona), anti-CD39 (B66, mIgG1 D265A, Tizona), anti-CD73 (2C5; mIgG1, Tizona), anti-PD-1 (RMP1-14), A2AR inhibitor (SCH58261; Sigma-Aldrich) with schedules and doses as indicated in the figure legends. For human tumor models, some groups of mice were treated with either cIg (palivizumab hG4, MedImmune), anti-human CD39 (TTX-030; Tizona), anti-PD-1 (pembrolizumab; Merck) with schedules and doses as indicated in the figure legends. No macroscopic signs of toxicity or weight change were detected after anti-CD39 therapy (data not shown).

Flow Cytometry

Tumors, tumor-draining lymph nodes, and spleens were harvested from mice untreated or treated with control or therapeutic antibodies as indicated in the figure legends. Tumors and lymph nodes were minced and digested with 1 mg/mL collagenase IV (Worthington Biochemical) and 0.02 mg/mL DNase I (Roche) and homogenized to prepare single-cell suspensions. Single-cell suspensions of spleens were depleted of erythrocytes. For surface staining, cells were stained in phosphate-buffered saline containing 2% (v/v) FBS with anti-CD45.2 (104; BD Biosciences) or anti-CD45.2 (30-F11; Thermo Fisher), anti-CD4 (RM4-5; BioLegend) or anti-CD4 (GK1.5; eBioscience), anti-CD8a (53-6.7; BioLegend), anti-TCR β (HS7-597; BioLegend), anti-NK1.1 (PK136; BD Biosciences), anti-CD39 (Duha59;

BioLegend), anti-CD73 (TY/23; BD Biosciences), OVA-tetramer (assembled with biotinylated KbOVA monomer from Professor Andrew Brooks Lab, the University of Melbourne and streptavidin from BD Biosciences), anti-CD279 (29F.1A12; BioLegend), anti-Ly6G (1A8; BioLegend), anti-CD11b (M1/70; BioLegend), anti-CD11c (N418; eBioscience), anti-CD64 (X54-5/7.1; BioLegend), anti-MHC II (M5/114.15.2; eBioscience), anti-CD274 (10F.9G2; BioLegend), and anti-P2X7R (1F11; BioLegend). For intracellular staining, surface-stained cells were fixed and permeabilized using the FOXP3/Transcription Factor Staining Buffer Set (eBioscience) or BD Cytotfix/Cytoperm (BD Biosciences) according to the manufacturer's protocol and stained with anti-FOXP3 (FJK-16s, eBioscience), anti-IFN γ (XMG1.2; BioLegend), anti-Ki-67 (16A8; BioLegend) or anti-Ki-67 (B56; BD Biosciences), and respective isotype antibodies. For intracellular staining of IFN γ , cells were stimulated *ex vivo* with eBioscience Cell Stimulation Cocktail (plus protein transport inhibitors) for 4 hours before surface staining. Populations defined in CD45⁺ live cells: CD8⁺ T cells, TCR β ⁺CD8⁺; CD4⁺FOXP3⁻ T cells, TCR β ⁺CD4⁺FOXP3⁻; Tregs, TCR β ⁺CD4⁺FOXP3⁺; NK cells, NK1.1⁺TCR β ⁻; neutrophils, Ly6G⁺; eosinophils, Ly6G⁻CD64⁺MHCII⁻CD11b⁺SSC^{hi}; macrophages, Ly6G⁻CD64⁺MHCII⁺; DCs, Ly6G⁻CD64⁺MHCII⁺CD11c⁺; and monocytes, Ly6G⁻CD64^{lo}MHCII^{lo}CD11b^{hi}SSC^{lo}. Cells were acquired on the BD LSRFortessa V (BD Biosciences), and analysis was carried out using FlowJo (Tree Star). Dead cells stained by 7-AAD (BioLegend) or Zombie Aqua (BioLegend) were excluded from analysis. Lymphoid and myeloid components were gated by markers indicated in Fig. S7.

IHC

IHC for CD8, CD39, PD-1, and CD19 staining was performed on mouse tumors harvested at the endpoint (day 23), in 10% neutral buffered formalin. Tumor sections were cut at 3 μ m onto superfrost+ glass slides and stored under vacuum until IHC was performed. Antibody-specific IHC conditions are listed in Supplementary Table S2. Briefly, antigen retrieval was done using a pressure decloaker (100°C; 20 minutes), and IHC was performed on a Dako Autostainer. Targets were visualized using the MACH3 HRP polymer detection system (Biocare; M3R531) and DAB Chromogen Kit (Biocare; BDB2004). Slides were counterstained with diluted hematoxylin and scanned using the 20 \times object lens on an Aperio AT system (Leica Biosystems). Representative images per tumor were captured using ImageScope software (Leica Biosystems).

Immunoblots

LPS-primed bone marrow-derived macrophages were stimulated with ATP for 90 minutes. Proteins in total cell lysates (prepared by RIPA buffer) and supernatants were detected by following mAbs: caspase-1 p20 (Casper-1, AdipoGen Life Science), anti-IL1 β (3A6, Cell Signaling Technology), and β -actin (13E5, Cell Signaling Technology).

RNA-seq

WT mice were injected subcutaneously with MC38 colon adenocarcinoma cells on day 0. Mice were treated *i.p.* with B66 or cIg (200 μ g) on day 12 and tumor samples were harvested 48 hours after treatment, followed by snap-freezing by dry ice. RNA isolation was performed using the RNeasy Mini Kit (Qiagen), and RNA samples with RIN > 7 were selected for cDNA library preparation using TruSeq RNA-seq using the Illumina (NextSeq 550) platform. A minimum of 27 million 76-bp paired-end reads were generated per sample. Sequence reads were trimmed for adapter sequences using Cutadapt (version 1.9; ref. 65) and aligned using STAR (version 2.5.2a; ref. 66) to the *Mus musculus* GRCm38 (MM10) reference genome assembly using the gene, transcript, and exon features model of Ensembl (release 70). Quality-control metrics were computed using RNA-SeQC (version 1.1.8; ref. 67), and transcript abundances were quantified using RSEM (version 1.2.30; ref. 68). Further analyses of

the RNA-seq data were carried out in R (version 3.5.1; <https://www.R-project.org/>). Protein-coding genes with <3 counts per million in fewer than 5 samples were removed from downstream analyses. Trimmed mean of M-values (TMM) normalization and differential gene-expression analysis were performed using the edgeR package (69). The “prcomp” function in R was used to perform principal component analysis on gene-wise centered and scaled values of TMM normalized expression data. Heat maps were produced using “ComplexHeatmap” R package (70) using gene-wise centered, scaled, log₂ values of TMM normalized expression data, and “pearson” distance with “ward.D” criteria to cluster the rows. GSEA was performed using the “fgsea” R package (71). RNA-seq data have been deposited in the European Nucleotide Archive (accession number: PRJEB32653).

Statistical Analysis

Statistical analysis was conducted with GraphPad Prism 7 (GraphPad Software). A one-tailed Mann-Whitney *U* test was used for comparisons of two groups. Significance of differences was also calculated by the log-rank *t* test for Kaplan-Meier survival analysis or two-way ANOVA as necessary. Tukey multiple-comparison tests were utilized unless otherwise indicated. A Fisher exact test was also used to determine significance of the proportion of tumor-free mice. Differences between groups are shown as the mean \pm SEM. *P* values of less than 0.05 were considered statistically significant.

Disclosure of Potential Conflicts of Interest

A.K. Moesta is Director, Immunology, at Tizona Therapeutics and has ownership interest (including patents) in the same. C. Wong is Associate Scientist, Antibody Discovery, at Tizona Therapeutics. T. dela Cruz is a scientist at Tizona Therapeutics and has ownership interest (including patents) in the same. M. Welch is an associate scientist at Tizona Therapeutics. A.G. Lerner is a senior principal scientist at Tizona Therapeutics. B.N. Spatola is a senior scientist at Tizona Therapeutics, Inc. V.B. Soros is Associate Director, Antibody Discovery, at Tizona Therapeutics and has ownership interest (including patents) in the same. J. Corbin is SVP, Antibody Development, at Tizona Therapeutics and has ownership interest (including patents) in the same. A.C. Anderson is a scientific advisory board member for Tizona Therapeutics, Zumutor Biologics, Compass Therapeutics, and Astellas Global Pharma. N. Waddell has ownership interest (including patents) in genomiQa and is an unpaid consultant/advisory board member for the same. C. Smith is a consultant at Atara Biotherapeutics and reports receiving a commercial research grant from the same. T. Bald is a scientific advisory board member for Oncomyx and reports receiving a commercial research grant from ENA Therapeutics. C. Beers is CSO at Tizona Therapeutics and has ownership interest (including patents) in the same. M.J. Smyth is a scientific advisory board member for Tizona Therapeutics and Compass Therapeutics and reports receiving commercial research grants from Bristol-Myers Squibb and Tizona Therapeutics. No potential conflicts of interest were disclosed by the other authors.

Authors' Contributions

Conception and design: X.-Y. Li, A.K. Moesta, K. Nakamura, S.C. Robson, C. Beers, M.J. Smyth

Development of methodology: X.-Y. Li, K. Nakamura, A. Lepletier, M. Efferm, M. Hölzel, C. Smith, T. Bald, N. Geetha, C. Beers

Acquisition of data (provided animals, acquired and managed patients, provided facilities, etc.): X.-Y. Li, C. Xiao, K. Nakamura, M. Casey, H. Zhang, A. Roman Aguilera, A. Sundararajan, C. Jacobberger-Foissac, C. Wong, T. dela Cruz, M. Welch, A.G. Lerner, B.N. Spatola, V.B. Soros, J. Corbin, S.C. Robson, M.J. Smyth

Analysis and interpretation of data (e.g., statistical analysis, biostatistics, computational analysis): X.-Y. Li, A.K. Moesta, K. Nakamura, H. Zhang, J. Madore, A. Lepletier, C. Wong, T. dela Cruz, B.N. Spatola,

V.B. Soros, J. Corbin, R.L. Johnston, N. Waddell, N. Geetha, M.W.L. Teng, M.J. Smyth

Writing, review, and/or revision of the manuscript: X.-Y. Li, A.K. Moesta, K. Nakamura, T. dela Cruz, V.B. Soros, J. Corbin, M. Hölzel, R.L. Johnston, C. Smith, T. Bald, N. Geetha, C. Beers, M.W.L. Teng, M.J. Smyth

Administrative, technical, or material support (i.e., reporting or organizing data, constructing databases): M. Effern, M. Hölzel, N. Geetha, M.J. Smyth

Study supervision: A.K. Moesta, T. Bald, N. Geetha, M.J. Smyth

Other (reagent generation): A.C. Anderson

Acknowledgments

The authors wish to thank Liam Town and Brodie Quine for genotyping and maintenance and care of the mice used in this study. The authors wish to thank Andrew Wong for assistance with expression and purification of antibodies. M.J. Smyth was supported by a National Health and Medical Research Council (NH&MRC) Senior Principal Research Fellowship (1078671) and Program Grant (1132519) and a Melanoma Research Alliance grant. S.C. Robson was supported by NIH R21CA221702, R01DK108894, and DoD W81XWH-15-PRMRP-FPA. M.W.L. Teng was supported by an NH&MRC Career Development Fellowship (1159655) and Project Grant (1120887) and the Prostate Cancer Foundation of Australia and It's a Bloke Thing Foundation. Some of the work was supported by a scientific research agreement with Tizona Therapeutics. T. Bald was supported by an NH&MRC Early Career Research Fellowship (1124690) and Project Grant (1138757). K. Nakamura was supported by the Naito Foundation and an NHMRC Project Grant (1174363). M. Hölzel was supported by DFG GRK2168 and M. Effern by a scholarship within GRK2168.

The costs of publication of this article were defrayed in part by the payment of page charges. This article must therefore be hereby marked *advertisement* in accordance with 18 U.S.C. Section 1734 solely to indicate this fact.

Received May 18, 2019; revised September 4, 2019; accepted October 1, 2019; published first November 7, 2019.

REFERENCES

- Smyth MJ, Ngiow SF, Ribas A, Teng MW. Combination cancer immunotherapy tailored to the tumour microenvironment. *Nat Rev Clin Oncol* 2016;13:143–58.
- Siu LL, Ivy SP, Dixon EL, Gravell AE, Reeves SA, Rosner GL. Challenges and opportunities in adapting clinical trial design for immunotherapies. *Clin Cancer Res* 2017;23:4950–8.
- Restifo NP, Smyth MJ, Snyder A. Acquired resistance to immunotherapy and future challenges. *Nat Rev Cancer* 2016;16:121–6.
- Pellegatti P, Raffaghello L, Bianchi G, Piccardi F, Pistoia V, Di Virgilio F. Increased level of extracellular ATP at tumor sites: in vivo imaging with plasma membrane luciferase. *PLoS One* 2008;3:e2599.
- Di Virgilio F, Falzoni S, Giuliani AL, Adinolfi E. P2 receptors in cancer progression and metastatic spreading. *Curr Opin Pharmacol* 2016;29:17–25.
- Takenaka MC, Robson S, Quintana FJ. Regulation of the T cell response by CD39. *Trends Immunol* 2016;37:427–39.
- Allard D, Turcotte M, Stagg J. Targeting A2 adenosine receptors in cancer. *Immunol Cell Biol* 2017;95:333–9.
- Eppell BA, Newell AM, Brown EJ. Adenosine receptors are expressed during differentiation of monocytes to macrophages in vitro. Implications for regulation of phagocytosis. *J Immunol* 1989;143:4141–5.
- Hasko G, Szabo C, Nemeth ZH, Kvetan V, Pastores SM, Vizi ES. Adenosine receptor agonists differentially regulate IL-10, TNF-alpha, and nitric oxide production in RAW 264.7 macrophages and in endotoxemic mice. *J Immunol* 1996;157:4634–40.
- Hasko G, Kuhel DG, Chen JF, Schwarzschild MA, Deitch EA, Mabley JG, et al. Adenosine inhibits IL-12 and TNF-[alpha] production via adenosine A2a receptor-dependent and independent mechanisms. *FASEB J* 2000;14:2065–74.
- Lappas CM, Rieger JM, Linden J. A2A adenosine receptor induction inhibits IFN-gamma production in murine CD4+ T cells. *J Immunol* 2005;174:1073–80.
- Minguet S, Huber M, Rosenkranz L, Schamel WW, Reth M, Brummer T. Adenosine and cAMP are potent inhibitors of the NF-kappa B pathway downstream of immunoreceptors. *Eur J Immunol* 2005;35:31–41.
- Deaglio S, Dwyer KM, Gao W, Friedman D, Usheva A, Erat A, et al. Adenosine generation catalyzed by CD39 and CD73 expressed on regulatory T cells mediates immune suppression. *J Exp Med* 2007;204:1257–65.
- Ohta A, Ohta A, Madasu M, Kini R, Subramanian M, Goel N, et al. A2A adenosine receptor may allow expansion of T cells lacking effector functions in extracellular adenosine-rich microenvironments. *J Immunol* 2009;183:5487–93.
- Bastid J, Cottalorda-Regairaz A, Alberici G, Bonnefoy N, Eliaou JF, Bensussan A. ENTPD1/CD39 is a promising therapeutic target in oncology. *Oncogene* 2013;32:1743–51.
- Zhang B, Cheng B, Li FS, Ding JH, Feng YY, Zhuo GZ, et al. High expression of CD39/ENTPD1 in malignant epithelial cells of human rectal adenocarcinoma. *Tumour Biol* 2015;36:9411–9.
- Hayes GM, Cairns B, Levashova Z, Chinn L, Perez M, Theunissen JW, et al. CD39 is a promising therapeutic antibody target for the treatment of soft tissue sarcoma. *Am J Transl Res* 2015;7:1181–8.
- Kozciak K, Sevigny J, Robson SC, Siegel JB, Kaczmarek E. Analysis of CD39/ATP diphosphohydrolase (ATPDase) expression in endothelial cells, platelets and leukocytes. *Thromb Haemost* 1999;82:1538–44.
- Borsellino G, Kleinewietfeld M, Di Mitri D, Sternjak A, Diamantini A, Giometto R, et al. Expression of ectonucleotidase CD39 by Foxp3+ Treg cells: hydrolysis of extracellular ATP and immune suppression. *Blood* 2007;110:1225–32.
- Gu J, Ni X, Pan X, Lu H, Lu Y, Zhao J, et al. Human CD39(hi) regulatory T cells present stronger stability and function under inflammatory conditions. *Cell Mol Immunol* 2017;14:521–8.
- Limagne E, Euvrard R, Thibaudin M, Rebe C, Derangere V, Chevriaux A, et al. Accumulation of MDSC and Th17 cells in patients with metastatic colorectal cancer predicts the efficacy of a FOLFOX-bevacizumab drug treatment regimen. *Cancer Res* 2016;76:5241–52.
- Montalban Del Barrio I, Penski C, Schlausa L, Stein RG, Diessner J, Wockel A, et al. Adenosine-generating ovarian cancer cells attract myeloid cells which differentiate into adenosine-generating tumor associated macrophages—a self-amplifying, CD39- and CD73-dependent mechanism for tumor immune escape. *J Immunother Cancer* 2016;4:49.
- Thelen M, Lechner A, Wennhold K, von Bergwelt-Baildon M, Schlosser HA. CD39 expression defines cell exhaustion in tumor-infiltrating CD8(+) T cells—Letter. *Cancer Res* 2018;78:5173–4.
- Canale FP, Ramello MC, Nunez N, Araujo Furlan CL, Bossio SN, Gorosito Serran M, et al. CD39 expression defines cell exhaustion in tumor-infiltrating CD8(+) T cells. *Cancer Res* 2018;78:115–28.
- Simoni Y, Becht E, Fehlings M, Loh CY, Koo SL, Teng KWW, et al. Bystander CD8(+) T cells are abundant and phenotypically distinct in human tumour infiltrates. *Nature* 2018;557:575–9.
- Duhen T, Duhen R, Montler R, Moses J, Moudgil T, de Miranda NF, et al. Co-expression of CD39 and CD103 identifies tumor-reactive CD8 T cells in human solid tumors. *Nat Commun* 2018;9:2724.
- Zhao H, Bo C, Kang Y, Li H. What else can CD39 tell us? *Front Immunol* 2017;8:727.
- Sun X, Wu Y, Gao W, Enjyoji K, Csizmadia E, Muller CE, et al. CD39/ENTPD1 expression by CD4+Foxp3+ regulatory T cells promotes hepatic metastatic tumor growth in mice. *Gastroenterology* 2010;139:1030–40.
- Feng L, Sun X, Csizmadia E, Han L, Bian S, Murakami T, et al. Vascular CD39/ENTPD1 directly promotes tumor cell growth by scavenging extracellular adenosine triphosphate. *Neoplasia* 2011;13:206–16.

30. Sun X, Han L, Seth P, Bian S, Li L, Cszimadia E, et al. Disordered purinergic signaling and abnormal cellular metabolism are associated with development of liver cancer in Cd39/ENTPD1 null mice. *Hepatology* 2013;57:205–16.
31. Zhang H, Vijayan D, Li XY, Robson SC, Geetha N, Teng MWL, et al. The role of NK cells and CD39 in the immunological control of tumor metastases. *Oncoimmunology* 2019; 8:e1593809.
32. Bastid J, Regairaz A, Bonnefoy N, Dejou C, Giustiniani J, Laheurte C, et al. Inhibition of CD39 enzymatic function at the surface of tumor cells alleviates their immunosuppressive activity. *Cancer Immunol Res* 2015;3:254–65.
33. Li XY, Das I, Lepletier A, Addala V, Bald T, Stannard K, et al. CD155 loss enhances tumor suppression via combined host and tumor-intrinsic mechanisms. *J Clin Invest* 2018;128:2613–25.
34. Ngiow SF, Young A, Jacquelot N, Yamazaki T, Enot D, Zitvogel L, et al. A threshold level of intratumor CD8⁺ T-cell PD1 expression dictates therapeutic response to anti-PD1. *Cancer Res* 2015;75:3800–11.
35. Selby MJ, Engelhardt JJ, Johnston RJ, Lu LS, Han M, Thudium K, et al. Preclinical development of ipilimumab and nivolumab combination immunotherapy: mouse tumor models, *in vitro* functional studies, and cynomolgus macaque toxicology. *PLoS One* 2016;11:e0161779.
36. Teng MW, Ngiow SF, von Scheidt B, McLaughlin N, Sparwasser T, Smyth MJ. Conditional regulatory T-cell depletion releases adaptive immunity preventing carcinogenesis and suppressing established tumor growth. *Cancer Res* 2010;70:7800–9.
37. Uno T, Takeda K, Kojima Y, Yoshizawa H, Akiba H, Mittler RS, et al. Eradication of established tumors in mice by a combination antibody-based therapy. *Nat Med* 2006;12:693–8.
38. Ngiow SF, Loi S, Thomas D, Smyth MJ. Mouse models of tumor immunotherapy. *Adv Immunol* 2016;130:1–24.
39. Glodde N, Bald T, van den Boorn-Konijnenberg D, Nakamura K, O'Donnell JS, Szczepanski S, et al. Reactive neutrophil responses dependent on the receptor tyrosine kinase c-MET limit cancer immunotherapy. *Immunity* 2017;47:789–802.
40. Ferrari D, Pizzirani C, Adinolfi E, Lemoli RM, Curti A, Idzko M, et al. The P2X7 receptor: a key player in IL-1 processing and release. *J Immunol* 2006;176:3877–83.
41. Adinolfi E, Giuliani AL, De Marchi E, Pegoraro A, Orioli E, Di Virgilio F. The P2X7 receptor: a main player in inflammation. *Biochem Pharmacol* 2018;151:234–44.
42. Ghiringhelli F, Apetoh L, Tesniere A, Aymeric L, Ma Y, Ortiz C, et al. Activation of the NLRP3 inflammasome in dendritic cells induces IL-1beta-dependent adaptive immunity against tumors. *Nat Med* 2009;15:1170–8.
43. Hu B, Ren J, Luo Y, Keith B, Young RM, Scholler J, et al. Augmentation of Antitumor immunity by human and mouse CAR T cells secreting IL-18. *Cell Rep* 2017;20:3025–33.
44. Stagg J, Loi S, Divisekera U, Ngiow SF, Duret H, Yagita H, et al. Anti-ErbB-2 mAb therapy requires type I and II interferons and synergizes with anti-PD-1 or anti-CD137 mAb therapy. *Proc Natl Acad Sci U S A* 2011;108:7142–7.
45. Landsberg J, Kohlmeyer J, Renn M, Bald T, Rogava M, Cron M, et al. Melanomas resist T-cell therapy through inflammation-induced reversible dedifferentiation. *Nature* 2012;490:412–6.
46. Lerner AG KM, Welch M, dela Cruz T, Jones J, Wong C, Spatola B, et al. Targeting CD39 with a first-in-class inhibitory antibody prevents ATP processing and increases T-cell activation. [abstract] In: *Proceedings of the American Association for Cancer Research, AACR Annual Meeting 2019; 2019 Mar 29–Apr 3; Atlanta, GA. Philadelphia (PA): AACR; 2019. Abstract nr 5012 2019.*
47. Kashyap AS, Thelemann T, Klar R, Kallert SM, Festag J, Buchi M, et al. Antisense oligonucleotide targeting CD39 improves anti-tumor T cell immunity. *J Immunother Cancer* 2019;7:67.
48. Vijayan D, Young A, Teng MWL, Smyth MJ. Targeting immunosuppressive adenosine in cancer. *Nat Rev Cancer* 2017;17:709–24.
49. Ohta A. A metabolic immune checkpoint: adenosine in tumor microenvironment. *Front Immunol* 2016;7:109.
50. Chen L, Diao L, Yang Y, Yi X, Rodriguez BL, Li Y, et al. CD38-mediated immunosuppression as a mechanism of tumor cell escape from PD-1/PD-L1 blockade. *Cancer Discov* 2018;8:1156–75.
51. Sade-Feldman M, Yizhak K, Bjorgaard SL, Ray JP, de Boer CG, Jenkins RW, et al. Defining T cell states associated with response to checkpoint immunotherapy in melanoma. *Cell* 2018;175:998–1013.
52. Bonnefoy N, Bastid J, Alberici G, Bensussan A, Eliaou JF. CD39: A complementary target to immune checkpoints to counteract tumor-mediated immunosuppression. *Oncoimmunology* 2015;4:e1003015.
53. Kronlage M, Song J, Sorokin L, Isfort K, Schwerdtle T, Leipziger J, et al. Autocrine purinergic receptor signaling is essential for macrophage chemotaxis. *Sci Signal* 2010;3:ra55.
54. Chen Y, Corriden R, Inoue Y, Yip L, Hashiguchi N, Zinkernagel A, et al. ATP release guides neutrophil chemotaxis via P2Y2 and A3 receptors. *Science* 2006;314:1792–5.
55. Cekic C, Linden J. Purinergic regulation of the immune system. *Nat Rev Immunol* 2016;16:177–92.
56. Kroemer G, Galluzzi L, Kepp O, Zitvogel L. Immunogenic cell death in cancer therapy. *Annu Rev Immunol* 2013;31:51–72.
57. Sitkovsky MV, Hatfield S, Abbott R, Belikoff B, Lukashev D, Ohta A. Hostile, hypoxia-A2-adenosinergic tumor biology as the next barrier to overcome for tumor immunologists. *Cancer Immunol Res* 2014;2:598–605.
58. Jackson SW, Hoshi T, Wu Y, Sun X, Enjyoji K, Cszimadia E, et al. Disordered purinergic signaling inhibits pathological angiogenesis in cd39/Entpd1-null mice. *Am J Pathol* 2007;171:1395–404.
59. Schaefer U, Machida T, Broekman MJ, Marcus AJ, Levi R. Targeted deletion of ectonucleoside triphosphate diphosphohydrolase 1/CD39 leads to desensitization of pre- and postsynaptic purinergic P2 receptors. *J Pharmacol Exp Ther* 2007;322:1269–77.
60. Enjyoji K, Sevigny J, Lin Y, Frenette PS, Christie PD, Esch JS 2nd, et al. Targeted disruption of cd39/ATP diphosphohydrolase results in disordered hemostasis and thromboregulation. *Nat Med* 1999;5:1010–7.
61. Solle M, Labasi J, Perregaux DG, Stam E, Petrushova N, Koller BH, et al. Altered cytokine production in mice lacking P2X(7) receptors. *J Biol Chem* 2001;276:125–32.
62. Clausen BE, Burkhardt C, Reith W, Renkawitz R, Forster I. Conditional gene targeting in macrophages and granulocytes using LysM-cre mice. *Transgenic Res* 1999;8:265–77.
63. Smith C, Khanna R. Generation of cytotoxic T lymphocytes for immunotherapy of EBV-associated malignancies. *Methods Mol Biol* 2010;651:49–59.
64. Dasari V, Schuessler A, Smith C, Wong Y, Miles JJ, Smyth MJ, et al. Prophylactic and therapeutic adenoviral vector-based multivirus-specific T-cell immunotherapy for transplant patients. *Mol Ther Methods Clin Dev* 2016;3:16058.
65. Martin M. Cutadapt removes adapter sequences from high-throughput sequencing reads. *EMBnetJournal* 2011;17:10.
66. Dobin A, Davis CA, Schlesinger F, Drenkow J, Zaleski C, Jha S, et al. STAR: ultrafast universal RNA-seq aligner. *Bioinformatics* 2013;29:15–21.
67. DeLuca DS, Levin JZ, Sivachenko A, Fennell T, Nazaire MD, Williams C, et al. RNA-SeQC: RNA-seq metrics for quality control and process optimization. *Bioinformatics* 2012;28:1530–2.
68. Li B, Dewey CN. RSEM: accurate transcript quantification from RNA-Seq data with or without a reference genome. *BMC Bioinformatics* 2011;12:323.
69. Robinson MD, McCarthy DJ, Smyth GK. edgeR: a Bioconductor package for differential expression analysis of digital gene expression data. *Bioinformatics* 2010;26:139–40.
70. Gu Z, Eils R, Schlesner M. Complex heatmaps reveal patterns and correlations in multidimensional genomic data. *Bioinformatics* 2016;32:2847–9.
71. Sergushichev AA, Loboda AA, Jha AK, Vincent EE, Driggers EM, Jones RG, et al. GAM: a web-service for integrated transcriptional and metabolic network analysis. *Nucleic Acids Res* 2016;44:W194–200.

CANCER DISCOVERY

Targeting CD39 in Cancer Reveals an Extracellular ATP- and Inflammasome-Driven Tumor Immunity

Xian-Yang Li, Achim K. Moesta, Christos Xiao, et al.

Cancer Discov 2019;9:1754-1773. Published OnlineFirst November 7, 2019.

Updated version	Access the most recent version of this article at: doi: 10.1158/2159-8290.CD-19-0541
Supplementary Material	Access the most recent supplemental material at: http://cancerdiscovery.aacrjournals.org/content/suppl/2019/10/17/2159-8290.CD-19-0541.DC1

Cited articles	This article cites 70 articles, 23 of which you can access for free at: http://cancerdiscovery.aacrjournals.org/content/9/12/1754.full#ref-list-1
Citing articles	This article has been cited by 1 HighWire-hosted articles. Access the articles at: http://cancerdiscovery.aacrjournals.org/content/9/12/1754.full#related-urls

E-mail alerts	Sign up to receive free email-alerts related to this article or journal.
Reprints and Subscriptions	To order reprints of this article or to subscribe to the journal, contact the AACR Publications Department at pubs@aacr.org .
Permissions	To request permission to re-use all or part of this article, use this link http://cancerdiscovery.aacrjournals.org/content/9/12/1754 . Click on "Request Permissions" which will take you to the Copyright Clearance Center's (CCC) Rightslink site.